Bioactive Materials 28 (2023) 480–494

Contents lists available at ScienceDirect

Bioactive Materials

journal homepage: www.keaipublishing.com/en/journals/bioactive-materials

An ischemic area-targeting, peroxynitrite-responsive, biomimetic carbon monoxide nanogenerator for preventing myocardial ischemia-reperfusion injury

Jinyan Zhang [a,b,d,e,1], Liwei Liu [a,b,d,e,1], Zhen Dong [a,b,d,e,1], Xicun Lu [f], Wenxuan Hong [a,b,d,e], Jin Liu [a,b,d,e], Xiaoyi Zou [a,b,d,e], Jinfeng Gao [a,b,d,e], Hao Jiang [a,b,d,e], Xiaolei Sun [a,b,d,e], Kai Hu [a,b], Youjun Yang [f], Junbo Ge [a,b,c,d,e], Xiao Luo [g,**], Aijun Sun [a,b,c,d,e,*]

[a] Department of Cardiology, Zhongshan Hospital, Fudan University, China
[b] Shanghai Institute of Cardiovascular Diseases, Shanghai, China
[c] Institutes of Biomedical Sciences, Fudan University, Shanghai, China
[d] NHC Key Laboratory of Viral Heart Diseases, Shanghai, China
[e] Key Laboratory of Viral Heart Diseases, Chinese Academy of Medical Sciences, China
[f] State Key Laboratory of Bioreactor Engineering, Shanghai Key Laboratory of Chemical Biology, School of Pharmacy, East China University of Science and Technology, Shanghai, 200237, China
[g] Shanghai Engineering Research Center of Molecular Therapeutics and New Drug Development, School of Chemistry and Molecular Engineering, East China Normal University, Shanghai, China

ARTICLE INFO

Keywords:
Ischemia-reperfusion injury
Macrophage membrane
Mitochondria
Inflammation
Peroxynitrite

ABSTRACT

Myocardial ischemia-reperfusion (MI/R) injury is common in patients who undergo revascularization therapy for myocardial infarction, often leading to cardiac dysfunction. Carbon monoxide (CO) has emerged as a therapeutic molecule due to its beneficial properties such as anti-inflammatory, anti-apoptotic, and mitochondrial biogenesis-promoting properties. However, its clinical application is limited due to uncontrolled release, potential toxicity, and poor targeting efficiency. To address these limitations, a peroxynitrite ($ONOO^-$)-triggered CO donor (PCOD585) is utilized to generate a poly (lactic-co-glycolic acid) (PLGA)-based, biomimetic CO nanogenerator (M/PCOD@PLGA) that is coated with the macrophage membrane, which could target to the ischemic area and neutralize proinflammatory cytokines. In the ischemic area, local produced $ONOO^-$ triggers the continuous release of CO from M/PCOD@PLGA, which efficiently ameliorates MI/R injury by clearing harmful $ONOO^-$, attenuating the inflammatory response, inhibiting cardiomyocyte apoptosis, and promoting mitochondrial biogenesis. This study provides a novel insight into the safe therapeutic use of CO for MI/R injury by utilizing a novel CO donor combined with biomimetic technology. The M/PCOD@PLGA nanogenerator offers targeted delivery of CO to the ischemic area, minimizing potential toxicity and enhancing therapeutic efficacy.

1. Introduction

Reperfusion through percutaneous coronary intervention (PCI) is a widely employed technique to treat patients suffering from acute myocardial infarction (MI). However, while reperfusion of the ischemic myocardium is beneficial, it can also result in myocardial ischemia-reperfusion (MI/R) injury, leading to necrotic or apoptotic cardiomyocyte death and eventual heart failure [1,2]. The most effective therapeutic strategy to reduce and even prevent MI/R injury involves specifically targeting the area in a timely manner during its

Peer review under responsibility of KeAi Communications Co., Ltd.
* Corresponding author. Department of Cardiology, Zhongshan Hospital, Fudan University, Shanghai Institute of Cardiovascular Diseases, No. 1609 Xietu Road, District Xuhui, Shanghai, 200025, China.
** Corresponding author. Shanghai Engineering Research Center of Molecular Therapeutics and New Drug Development, School of Chemistry and Molecular Engineering, East China Normal University, Shanghai, 200241, China.
E-mail addresses: xluo@chem.ecnu.edu.cn (X. Luo), sun.aijun@zs-hospital.sh.cn (A. Sun).
[1] These authors have contributed equally to this work.

https://doi.org/10.1016/j.bioactmat.2023.05.017
Received 30 November 2022; Received in revised form 26 April 2023; Accepted 24 May 2023

pathogenesis.

Recent work has demonstrated that oxidative stress, inflammation, and mitochondrial dysfunction cause further damage to the myocardial ischemic tissues during reperfusion. Thus, more effective, rapid, and targeted strategies to ameliorate these three factors are urgently needed. Oxidative stress plays a crucial role in the development of MI/R injury. Following ischemia, reperfusion leads to the overproduction of superoxide anions [3]. These anions react with nitric oxide (NO) and form peroxynitrite (ONOO-) [4,5]. $ONOO^-$ is responsible for calcium (Ca^{2+}) pump impairment, apoptotic cell death, vascular endothelial dysfunction, and postoperative sequalae, such as atrial fibrillation and heart failure [6–9]. The cascade of inflammatory effects triggered by cardiomyocyte death is another factor that offsets the clinical benefits of reperfusion following myocardial infarction. This has been extensively studied, but therapeutic interventions are still lacking [10]. During reperfusion, patient outcomes are worsened by the excessive recruitment and uncontrolled activation of M1 macrophages. In fact, immunotherapy aimed to inhibit pro-inflammatory M1 macrophages and promote reparative M2 macrophages has been shown to attenuate postischemia inflammation and provide cardio-protection in a preclinical MI/R model [11–13]. Finally, oxidative stress also impairs the mitochondrial electron transport chain, which leads to a decrease in ATP synthesis and mitochondrial respiration. This, in turn, causes diastolic stiffness and contractile dysfunction [14,15]. Mitochondrial dysfunction caused by oxidative damage further hinders the recovery of cardiac function after reperfusion [16]. Therefore, ameliorating mitochondrial damage may offer a potential therapeutic strategy for treating MI/R [17].

Based on the above findings, mitochondrial dysfunction, inflammation, and excessive reactive oxygen species (ROS) generation all play a critical role in the pathogenesis of MI/R injury, but there is a lack of treatments that specifically target all three of these factors. Endogenous carbon monoxide (CO) generated from heme decomposition by heme oxygenase-1 (HO-1) has anti-apoptotic and anti-inflammatory properties [18]. Its beneficial impact on mitochondrial function has also been widely reported [19]. However, the application of CO for treating cardiovascular diseases is limited by its delivery system. Over the past decades, CO gas inhalation, CO in a liquid formulation, organic CO prodrugs, and metal-based CO-releasing molecules (CORMs) have been used as CO donors [20]. Recently, Cheng et al. have developed a photo-triggered CO donor to enhance wound healing [21]. Another study has used gas-entrapping materials to deliver CO to the gastrointestinal tract [22]. Despite their potential therapeutic benefits, CO donors have not been successful in achieving controlled release and targeted delivery in cardiovascular disease. As a result, there is an urgent need for the development of an innovative delivery system that can minimize adverse side effects of CO donors and increase their efficacy. This is crucial to facilitate their clinical application in cardiovascular disease.

This study introduces a novel CO donors delivery system, consisting of macrophage cell membrane-coated PLGA nanoparticles and PCOD585 (M/PCOD@PLGA). The system is designed to target the three major factors that drive MI/R injury: inflammation, mitochondrial dysfunction, and oxidative stress. By precisely targeting these factors, M/PCOD@PLGA provides a preventive strategy against MI/R injury. The study demonstrates that functional portions of the macrophage cell membrane coated onto the surface of PLGA nanoparticles promotes their delivery to the ischemic area. Additionally, because PCOD585 is an $ONOO^-$-responsive CO donor [23], it can react with harmful $ONOO^-$ and release CO simultaneously. CO alleviates inflammation, decreases cardiomyocyte apoptosis, and ameliorates mitochondrial dysfunction. Further investigation of the bioactivity and biodistribution of M/PCOD@PLGA in mice reveals that these biomimetic nanoparticles reduce infarction size, thus improving cardiac function after MI/R injury. Taken together, these findings suggest that M/PCOD@PLGA may be a promising therapeutic approach for preventing or treating MI/R injury.

2. Materials and methods

2.1. Preparation of macrophage membrane vesicles

Raw 264.7 cells were resuspended in 3 ml separation buffer (250 mM sucrose, 20 mM Tricine, 1 mM Ethylenediaminetetraacetic acid (EDTA) dissolved in ddH_2O). After centrifugation (4 °C, 1000 g, 5min), the precipitates were collected and resuspended in homogenization buffer (225 mM Mannose, 75 mM sucrose, 0.5% bovine serum albumin (BSA), 0.5 mM EDTA, 30 mM Tris(hydroxymethyl)methyl aminomethane THAM(Tris), protease and phosphatase inhibitor cocktail (Thermo Scientific™, 78440, 1:100) dissolved in ddH_2O). After being homogenized for 20–30 times, the sample was centrifugated (4 °C, 100000 g, 1 h) and the supernatant was removed. To obtain macrophage membrane vesicles, the precipitates were resuspended in ddH2O and extruded through polycarbonate membranes (Avanti, 610006, 610007) using a Avestin mini-extruder (Avestin, 610000).

2.2. Preparation of PCOD585-Loaded PLGA (PCOD@PLGA)

An emulsification process was used to prepare PCOD@PLGA nanoparticles [24]. Briefly, 3.6 mg PCOD585 was dissolved in 500 μl mixed solution (200 μl dimethyl sulfoxide (DMSO) +300 μl chloroform) and 100 mg PLGA-PEG-NH2 (100 mg) were dissolved into 2.2 ml chloroform. PCOD585 and PLGA solutions were mixed, followed by ultrasonic emulsification, and added to the aqueous phase (10 mL 1%PVA). The mixture was sonicated at 192 w for 4 min and stirred (100 rpm) for 12 h. The remaining solution was collected in a 100 kD ultra-filter tube and ultra-filtered for 15 min at 4 °C (EMD Millipore UFC910024). Then we collected and lyophilized the solutions of PCOD@PLGA nanoparticles for the following experiments.

2.3. Drug loading study

The lyophilized PCOD@PLGA powder was dissolved in DMSO and measured at 550 nM using a UV–vis spectrophotometer (Beckman Coulter, DU730). Using the pre-established PCOD585 standard curve, the loading and encapsulation efficiency was calculated as follows:

$$loading\ efficiency(\%) = \frac{Mass\ of\ PCOD585\ in\ \text{PCOD@PLGA}}{Mass\ of\ \text{PCOD@PLGA}} \times 100\%$$

$$\text{encapsulation efficiency}\ (\%) = \frac{Mass\ of\ PCOD585\ in\ \text{PCOD@PLGA}}{Mass\ of\ PCOD585\ in\ feed} \times 100\%$$

2.4. Preparation of macrophage membrane coating PCOD@PLGA(M/PCOD@PLGA)

Co-extrusion method was used to prepare M/PCOD@PLGA. Briefly, the harvested macrophage membrane vesicles (1 mg protein) were mixed with PCOD@PLGA (100 μg). Then, the mixture was ultrasonicated (100w, 2 min) on ice. Subsequently, the mixture solution was extruded for 10 times (400, 200 nm polycarbonate porous membrane successively) using an Avestin mini-extruder (Avestin, 610000, Canada).

2.5. Nanoparticles characterization

The zeta potential and size of PCOD@PLGA, M/PCOD@PLGA was measured by Malvern Zetasizer Nano ZS unit (Malvern, Nano ZS 90). Both transmission electron microscopy (TEM, JEOL JEM 2100F microscope) and scanning electron microscopy (SEM, Zeiss Sigma 300) was used to evaluate the morphology of nanoparticles.

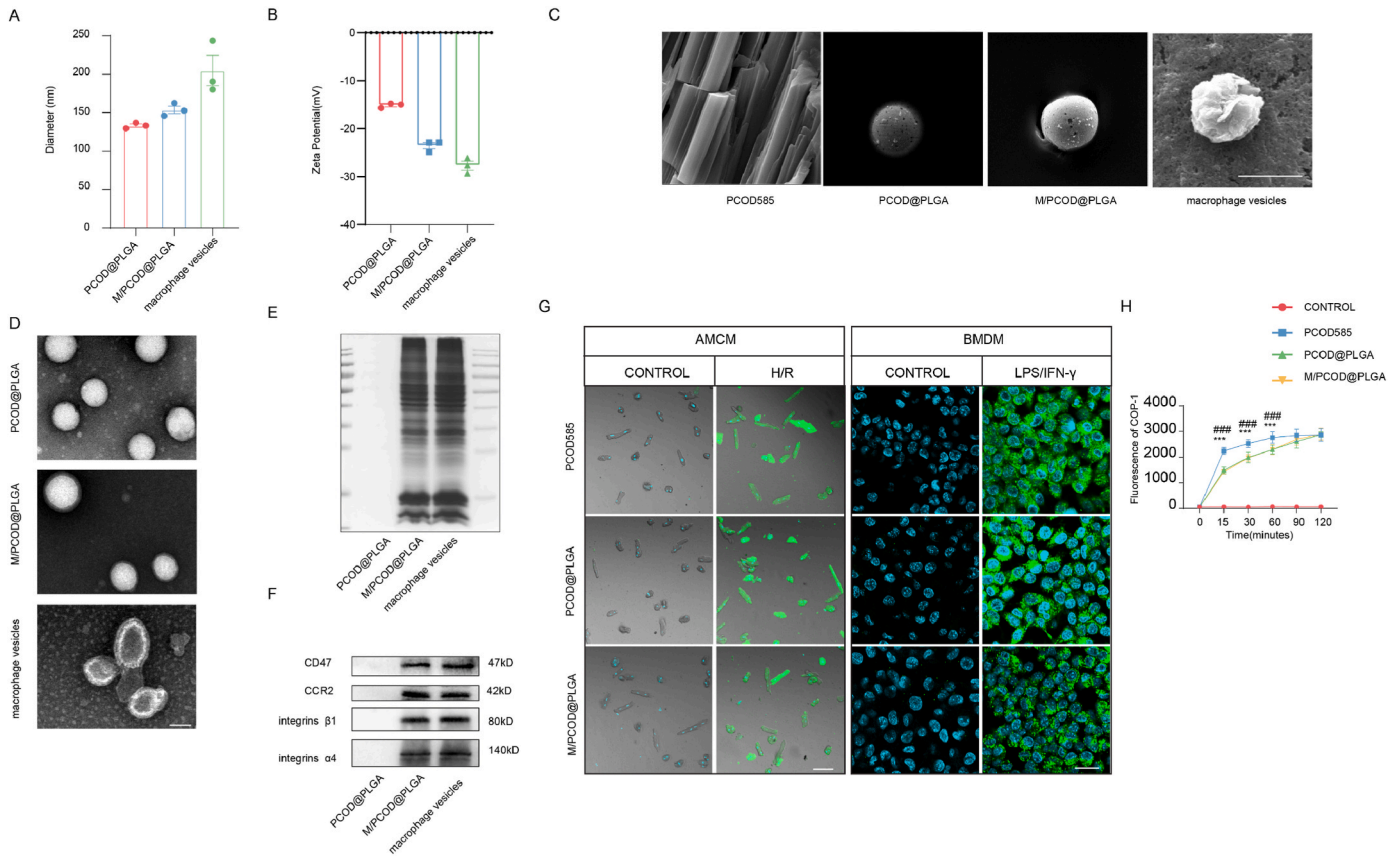

Fig. 1. In vitro characterization of M/PCOD@PLGA.
A) Particle sizes and B) Zeta potentials of PCOD@PLGA, M/PCOD@PLGA, and macrophage vesicles. C) SEM image of PCOD585 powder, PCOD@PLGA, macrophage vesicle and M/PCOD@PLGA. Scale bar: 200 nm. D)TEM image of PCOD@PLGA, macrophage vesicle and M/PCOD@PLGA. Scale bar: 100 nm. E) Gel images of the protein extracted from M/PCOD@PLGA, macrophage membranes and PCOD@PLGA, by Coomassie Blue Staining. F) Characteristic protein bands of macrophage membranes and PCOD@PLGA, M/PCOD@PLGA by Western blotting. G) CLSM imaging of CO in AMCMs an BMDMs treated in different groups. Scale bar: 100 μm (left), 20 μm(right). H) Cumulative CO release from PCOD585, PCOD@PLGA, M/PCOD@PLGA cocultured with SIN-1. (n = 8) (* VS PCOD@PLGA; # vs M/PCOD@PLGA, ***: $p < 0.001$, ###$p < 0.001$.).

2.6. Western blot assay

For extracting protein from cell, cells were washed by PBS and then lysed by RIPA lysis. After centrifugation (12000 rpm, 15 min), supernatant was collected. For extracting protein from heart tissue, hearts were perfused with 5 ml PBS to remove blood. Then, heart was removed from the chest cavity and be cut into small pieces. The tissues were ground in ice cold RIPA buffer. After centrifugation (12000 rpm, 15 min), supernatant was collected in another tube. The BCA assay kit (Beyotime, P0010S) was applied for detecting protein concentrations of supernatant. Then, the supernatant was mixed with SDS-PAGE Sample Loading Buffer (Beyotime, P0015). Proteins were separated in SDS/PAGE gels. To evaluate protein of macrophage membrane, PCOD/PLGA and M/PCOD@PLGA, the membrane proteins was run on 12% gel and stained with Coomassie Blue (Beyotime, P0017F). For detecting other proteins, the protein was transferred to PVDF membrane after electrophoresis. Then, we blocked the membrane with 5% BSA and incubated it with indicated antibodies against the different proteins. After incubating with indicated antibody for 12 h (at 4 °C), the PVDF membrane was washed by TBST (TBS with Tween-20) (Beyotime, ST673) solution for 3 times (10 min each) and incubated with secondary antibody for 1.5 h (room temperature). After being washed with TBST (3 times, 10 min each), the PVDF membrane was developed with enhanced chemiluminescence (ECL).

2.7. Detection of CO in vitro

CO Probe 1 (COP-1) was prepared as previously described [25]. For assess the CO release rate triggered by $ONOO^-$, PCOD585 (500μM), PCOD/PLGA (at a dose of 500 μM PCOD585) and M/PCOD@PLGA (at a dose of 500 μM PCOD585) was mixed with 50uM 3-Morpholino Sydnonimine Hydrochloride (SIN-1), then 10uM COP-1 was added to the above solution. The fluorescent was read at each time point with a microplate reader. (λ_{ex} = 475 nm, λ_{em} = 510 nm). For intracellular CO detection, cells were co-cultured with 1uM COP-1 after receiving indicated intervention. Then, cells were stained with Hoechst 33342 visualized under the confocal laser scanning microscope (CLSM) (OLYMPUS, FLUOVIEW FV3000).

2.8. Evaluation of $ONOO^-$ in vitro and in vivo

The $ONOO^-$ levels of cells were detected by $ONOO^-$ Assay Kit (Bestbio, BB-46065). The $ONOO^-$ levels of heart tissues were detected by Slice $ONOO^-$ detection kit (Bestbio, BB-46085). After being stained by following steps recommended by the kit, the fluorescence was visualized by the CLSM.

2.9. Tunel staining

After receiving indicated intervention, apoptosis levels of mice tissues and cells were measured by One Step TUNEL Apoptosis Assay Kit (Beyotime, C1086). The fluorescence signal of apoptotic cells and heart

tissues was detected by CLSM.

2.10. RNA extraction and quantitative reverse transcription-PCR(RT-qPCR)

TRIzol reagent (Invitrogen, 15596026CN) was applied for extracting RNA from mouse tissue or cultured cells. Then, the RNA was reverse transcribed into cDNA by using RT Master Mix (Takara, RR036A). To quantify the expression levels of the target gene, we performed real-time quantitative PCR (RT-qPCR) using SYBR qPCR Master Mix (Vazyme, Q712-02) on the CFX Connect system (Bio-Rad). Expression levels of gene were normalized using the ΔΔCT method relative to *18S* ribosomal RNA levels.

2.11. Adult mice cardiomyocytes (AMCMs) isolation and hypoxia/reoxygenation(H/R)

AMCMs were isolated and cultured as previously described [26]. For in vitro experiments, mice were anesthetized with pentobarbital and the thoracic and abdominal cavity was opened. After excision of the abdominal aorta, 6 ml EDTA buffer were injected into the right ventricle in 1 min. Then, we blocked the aortic arch using vessel clamp and transferred the heart to the dishes. 20 ml EDTA buffer, 6 ml perfusion buffer, and 40 ml enzyme mixture solution were successively injected into the left ventricle. Then, we dissected the heart into 1 mm^3 pieces with forceps and the cell suspension were flowed through a 100 μM cell strainer. After sedimentation for 20 min, AMCMs were precipitated at the bottom. After the gradient recovery of the calcium concentration, AMCMs were plated on the laminin-coated dish and prepared for further research. To induce hypoxia/reoxygenation(H/R) injury, AMCM was cultured with hypoxic solution (NaH2PO4 0.9 mmol/L, CaCl2 1 mmol/L, MgSO4 1.2 mmol/L, HEPES 20 mmol/L, NaHCO3 6 mmol/L, KCL 10 mmol/L, NaCl 98.5 mmol/L, Sodium lactate 40 mmol/L, adjusted to PH 6.8) (with 10 ng/ml TNF-α) at 1% O2 for 1 h, subsequently replaced hypoxic solution with culture media and then culture AMCMs at 21% O2 for 4 h.

2.12. Operation and analysis of MI/R injury in mice

The animal ethics committee approved all procedures in compliance with the NIH Guide for Animal welfare (no. 85–23, revised 1996). For MI/R injury [14], 8 weeks-old male C57BL6/J mice were anesthetized using 2% isoflurane. MI/R was executed by exposing the heart through a left thoracotomy. The left anterior descending coronary artery was temporally tied by a slipknot. ST-segment elevation on electrocardiogram confirmed successful coronary occlusion. We released the slipknot after 45-min ischemia. Then, myocardial reperfusion commenced for indicated time. After operation, mice were randomized to control (5% DMSO, 5% Tween 80, 40% PEG300, 50% PBS or PBS), PCOD585 (6 mg/kg), PCOD@PLGA (at a dose of 6 mg/kg PCOD585), M/PCOD@PLGA (at a dose of 6 mg/kg PCOD585) treatment group. Echocardiography (Visual Sonic VeVo 2100, Canada) was performed to evaluate the cardiac function. To assess the infarct size of heart, Evans's blue was injected retrogradely through the aortic root to demarcate the nonischemic/reperfused area and heart tissues were stained using 1% 2, 3,5-triphenyltetrazolium chloride (TTC) solution. Then, TTC-negative (pale) infarcted regions could be easily distinguished from TTC-positive viable cardiac regions by brick red staining. The scar size and fibrosis size of heart was determined by Masson and Sirius Red staining as previously described.

2.13. Assessment of cell viability

Cell Counting Kit-8 (Beyotime, C0038) was used to evaluate cell viability of AMCMs. The absorbance at 450 nm was measured.

2.14. Nanoparticles uptake by cells

After receiving indicated interventions, Cy5.5@PLGA and M/Cy5.5@PLGA were added and incubated for indicated periods. The cells were washed with PBS, fixed by 4% paraformaldehyde, stained using DAPI for 15 min, and observed via CLSM. To block Integrin α4 and Integrin β1, M/Cy5.5@PLGA were incubated with anti-Integrin α4 and anti-Integrin β1 antibody at 37 °C for 20 min. Fluorescent intensity was analyzed with Image J software.

2.15. In vivo targeting of the ischemic heart

After subjected to MI/R injury, Cy5.5@PLGA and M/Cy5.5@PLGA were injected to mice via tail vein. Mice were euthanized 6 h later. In order to remove unbound dyes, hearts of these mice subsequently perfused with PBS. The liver, heart, lung. spleen, and kidney imaged and analyzed by IVIS®LuminaIII system. To assess the distribution of nanoparticles by fluorescence microscopy, hearts were embedded in OCT cryo-embedding compound immediately after excision from body. After staining with the corresponding primary and secondary antibodies, the frozen sections observed under CLSM. Fluorescent intensity was analyzed with Image J software.

2.16. Seahorse assay

AMCMs were isolated from mice received with different treatment and were plated in Seahorse 96-well plate. Then, oxygen consumption rate (OCR) was exaluated through the XFe96 extracellular flux analyzer (Seahorse Bioscience).

2.17. ATP measurements

ATP levels of mice tissues was measured by ATP Assay Kit (Beyotime, S0027). 20 mg freshly harvested heart tissue were lysed by lysis buffer. To prepare ATP standard solutions, ATP solution (0.5 mM) was diluted in ATP detection reagent dilution. Standards solution and samples were added to 96 Well Assay Plate (Corning Incorporated, 3603). Luminescence was detected by luminometer. ATP amount was calculated against a standard curve.

2.18. Transmission electron microscopy

The heart tissues were prepared for transmission electron microscopy by first dissecting them into small cubes with a size of 1mm3 or less. The samples were then fixed with 2.5% glutaraldehyde at pH 7.4, followed by fixation with 1% osmium tetroxide in 0.1 M PBS at pH 7.4. After fixation, the tissues were dehydrated using graded series of ethanol (30%, 50%, 70%, 80%, 95%, and 100%) and then sequentially treated with acetone: 812 embedding agent (1:1) for 4 h, acetone: 812 embedding agents (1:2) overnight, and 812 embedding agent for 8 h. Finally, the tissues were baked at 60 °C for 48 h. Ultrathin sections of 60 nm thickness were prepared from the embedded tissues and stained with 2% uranyl acetate for 8 min and 2.6% lead citrate for 8 min. The prepared samples were examined using a Hitachi HT7800/HT7700 transmission electron microscope. Qualitative analysis was performed by collecting at least six fields per mouse to obtain representative images.

2.19. Safety evaluation

Eight-week-old mice were injected with different formulations of PCOD585 (at the same dose described above) to assess biosafety of these formulations in vivo. For histological study, mice were sacrificed and their serum, brains, kidneys, spleens, lungs, and, livers were collected. Liver and kidney function biomarkers (ALT, AST, and creatinine) were measured by indicated kits (ALT assay kit (Nanjing Jiancheng, C009-2-1); AST assay kit (Nanjing Jiancheng, C010-2-1); creatinine assay kit

(Nanjing Jiancheng, C011-2-1).

2.20. Isolation of BMDMs

Immediately after euthanasia, the femora and tibiae of mice were collected and place in 4 °C PBS. Then, the femora and tibiae were flushed with PBS to harvest cells. After filtration through 100 μm strainers, we further lysed red blood cells. By co-cultured with macrophage colony-stimulating factor (M-CSF) (10 ng/ml) for 7 days, total bone marrow cells would differentiate into BMDMs. To induce macrophage polarization, BMDMs were treated with (LPS 100 ng/ml + IFN-γ 20 ng/ml) for 12 h.

2.21. Blood gas analysis

Blood was collected in BD Vacutainer® EDTA Tubes (BD, 367863) at 48 h after treatment. The blood samples were run on blood gas analyzers (Roche, cobas b 123).

2.22. Tissue CO analysis

Analysis of CO concentration of heart tissues was based on previous methods [27]. The hearts were perfused with ice-cold KH2PO4 buffer (pH 7.4) and collected in a centrifuge tube stored on ice. Subsequently, the heart was placed in water, chopped with surgical scissors, homogenized with a tissue grinder, and then sonicated on ice (10 W, 8 to 10 1-s pulses). A borosilicate glass chromatography vial (2 ml) with a silicone septum was prepared. Then, 10 μl homogenate were mixed with 20 μl 20% Sulfosalicylic acid (SSA) and mixture was injected into amber vials through a gas-tight syringe. Then, the CO released from mixture was delivered into gas chromatography system by diverting the CO-free carrier gas through the vial headspace. The peak area was measured. Besides, standard CO gas was used to generate a standard curve.

2.23. LPS and cytokine binding in vitro

To study the binding ability of M/PCOD@PLGA, M/PCOD@PLGA (at a concentration of 1 μM M/PCOD@PLGA) or PCOD@PLGA (at a concentration of 1 μM M/PCOD@PLGA) was respectively mixed with LPS (100 ng/ml), IL-6 (500 pg/ml), TNF-α (500 pg/ml), IFN-γ (500 pg/ml). After incubating for 2 h at 37 °C, the mixture was subjected to centrifugation at 16,000 g for 10 min. Following this, the LPS concentration in the supernatant was determined using an LPS assay kit (Thermo Scientific™, A39552). IL-6, TNF-α and IFN-γ concentration was evaluated by ELISA kit (abclonal).

2.24. Drug release profile in vitro

We added M/PCOD@PLGA and PCOD@PLGA solutions to disposable dialysis cups (Thermo Scientifc, MWCO:3500 Da) in drug release buffer (PBS with 5% DMF, PH = 7.4). At several time points (1, 2, 12, 24, 48, 72 h), the external buffers were collected and equal fresh drug release buffer was added. High performance liquid chromatography (HPLC) was applied for calculating the amount of PCOD585 released.

2.25. In vivo pharmacokinetics study

8-week-old male mice with similar weight was used in this experiment. Cy5.5@PLGA and M/Cy5.5@PLGA (contain same amount of Cy5.5) was administrated to the mice (via tail vein). At different time points after injection (3min, 1 h, 4 h, 12 h, 24 h), 20 μl of blood was collected from tail vein. 40 μl PBS (with EDTA) was added to the blood samples. Then, we transferred the mixture to 96-well plates. The fluorescence of mixture was detected by microplate reader.

2.26. Statistical analysis

All data were reported as means with standard error of the mean (SEM). Normality was evaluated by Shapiro-Wilk test. To compare between two groups (variances are equal), we applied a *t*-test. To compare between two groups (variances are not equal), we applied unpaired *t*-test with Welch's correction. For comparisons involving three or more groups (variances are equal), we used a one-way ANOVA followed by Tukey's post hoc test. For comparisons involving three or more groups (variances are not equal), we used Welch's ANOVA test followed by Games-Howell post-hoc test. NS no significance, *: $p < 0.05$, **: $p < 0.01$, ***: $p < 0.001$. In our study, Cohen's d, Glass's delta, and Hedges' g were applied for calculating effect size. When variances are not significantly different, Cohen's d (total sample sizes are over or equal to 20) and Hedges' g (total sample sizes are below 20 or sample sizes are unequal) were applied for calculating effect sizes. When variances are significantly different, Glass's delta was applied for calculating effect size. Rank of effect size: small effect = 0.2 medium effect = 0.5, large effect = 0.8 [28] (Table S4).

3. Results

3.1. Preparation and characterization of M/PCOD@PLGA

The synthetic pathway and reaction mechanism of PCOD585 were described in Fig. S1. The drug loading content (DLC) of PCOD@PLGA was 5.69%, and its encapsulation efficiency was 89.7% (Table S1). M/PCOD@PLGA was prepared by co-extrusion method, as previously described, using the extracted macrophage vesicles [29]. The hydrodynamic diameter (Dh) of M/PCOD@PLGA was determined to be 153.7 ± 4.788 nm by dynamic light scattering (DLS) measurements, approximately 20.6 nm larger than PCOD@PLGA (Fig. 1A). M/PCOD@PLGA exhibited homogeneous dispersity and high uniformity in size (mean polydispersity index [PDI] = 0.194 ± 0.047). The PCOD@PLGA was stable in both PBS and serum for at least 3 days (Fig. S2). Additionally, the surface zeta potential at room temperature of M/PCOD@PLGA was −23.57 ± 1.155 mV (Fig. 1B). As shown in Fig. 1C, scanning electron microscopy (SEM) images indicated that both PCOD@PLGA and M/PCOD@PLGA are spherical, while the PCOD585 powder had a clear crystal structure. The morphology of macrophage vesicle, PCOD@PLGA and M/PCOD@PLGA was also observed via transmission electron microscopy (TEM). As shown in Fig. 1D, the M/PCOD@PLGA exhibited a distinctive spherical core-shell structure (PCOD@PLGA "core" and a macrophage membrane "shell"). The protein profiles of M/PCOD@PLGA were close to those of macrophage membrane vesicles (Fig. 1E), suggesting that the prepared nanoparticles successfully retained almost all membrane proteins from BMDMs. M/PCOD@PLGA was further subjected to western blot analysis to verify expression of some important proteins, which mediates macrophage accumulated in injured cardiac tissue. Indeed, the successful expression of integrin α4β1, C–C chemokine receptor type 2 (CCR2) and CD47 proteins on the surface of M/PCOD@PLGA was demonstrated (Fig. 1F). These findings indicated that the PCOD5@PLGA surface was successfully coated with the macrophage membrane. The ability of PCOD@PLGA and M/PCOD@PLGA to release PCOD585 was next examined. As shown in Fig. S3, PCOD585 was released from PCOD@PLGA and M/PCOD@PLGA gradually over time.

The $ONOO^-$-induced CO release of PCOD585, PCOD@PLGA, and M/PCOD@PLGA was next examined using a fluorogenic CO probe 1 (COP-1). Strong green fluorescence was visualized in hypoxia/reoxygenation (H/R)-treated AMCMs and lipopolysaccharide/interferon-gamma (LPS/IFN-γ)- BMDMs (Fig. 1G), whereas no fluorescence was observed in untreated cells. Next, fluorescence (emission at 520 nm) was measured to calculate the release of CO. We respectively mixed PCOD585 (500 μM), PCOD@PLGA (at a dose of 500 μM PCOD585), M/PCOD@PLGA (at a dose of 500 μM PCOD585) with 50 μM SIN-1 (could produce 50 μM

ONOO-). A rapid rise in CO plateaued at 15 min in the PCOD585 group. However, CO was steadily released over a duration of 30 min to 2 h in the PCOD@PLGA and M/PCOD@PLGA groups. In the end, the releasing curve of all three group was no longer rising, since the $ONOO^-$ is total eliminated (Fig. 1H). Overall, these results indicated that PCOD@PLGA and M/PCOD@PLGA were an ideal CO donor for the sustained delivery and controlled release of CO.

3.2. Therapeutic effects of M/PCOD@PLGA in vitro

The safety of M/PCOD@PLGA was first tested in BMDMs, human umbilical vein endothelial cells (HUVECs), and AMCMs. No obvious cytotoxicity was observed (Figs. S4A and B). MI/R injury included two periods: ischemia period and subsequent reperfusion period. During ischemia period, occlusion of coronary artery leads to insufficient blood supply for cardiomyocytes, which make cardiomyocyte unable to access enough oxygen and nutrients. During reperfusion period, sudden restoration of blood and oxygen supply would cause further damage to cardiomyocyte [2]. Thus, AMCMs subjected to hypoxia/reoxygenation was selected as in vitro model to mimic the cardiomyocyte damage during MI/R injury. Then, macrophage originated from bone marrow would infiltrate into the injured myocardium and polarized into M1 (pro-inflammatory) phenotype in early stage of MI/R injury [11]. Thus, BMDMs treated with LPS/IFN-γ was selected as in vitro model to

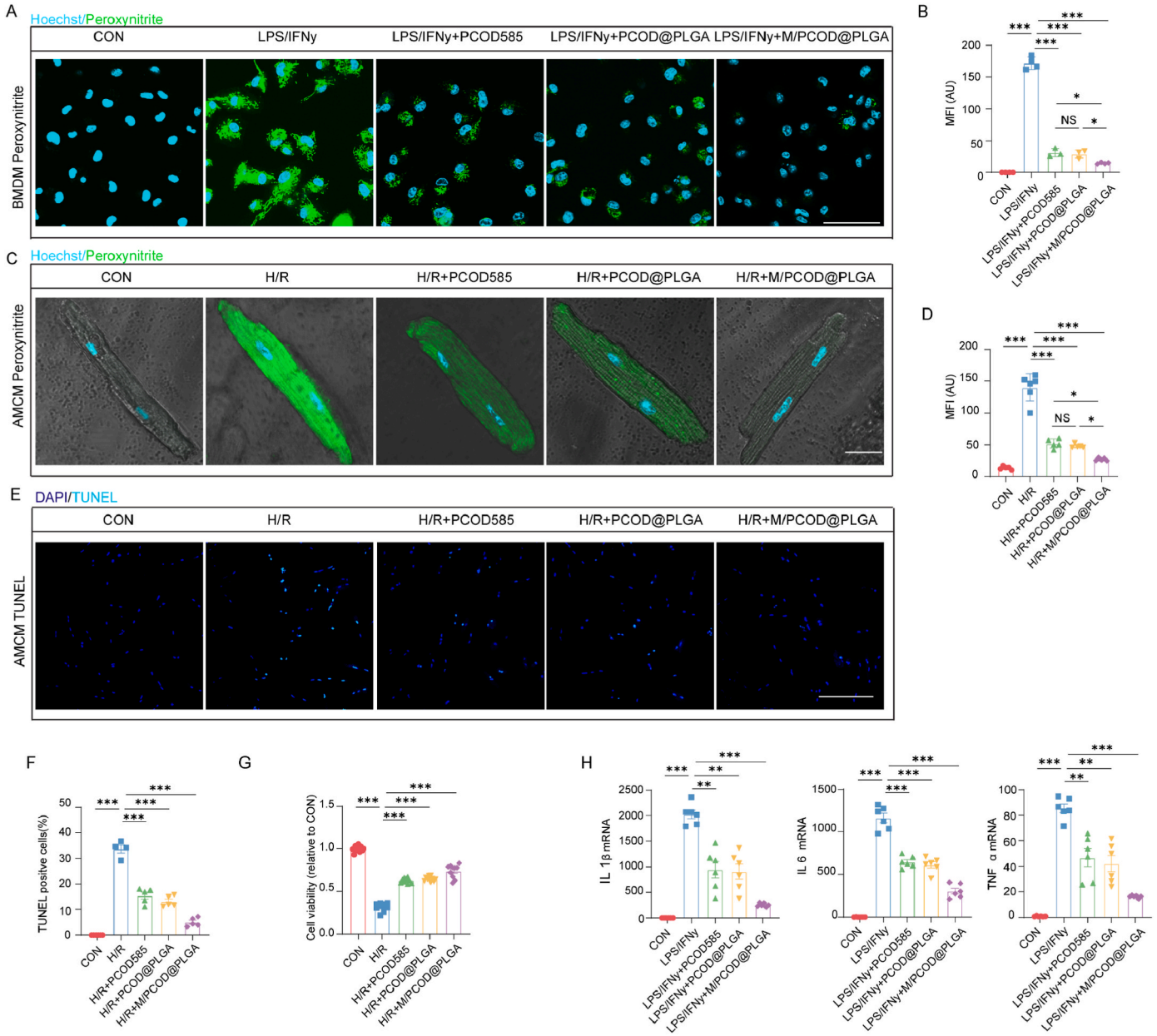

Fig. 2. Scavenge ability of $ONOO^-$ and attenuation effects of inflammation of PCOD585, PCOD@PLGA, M/PCOD@PLGA in vitro.
A) CLSM imaging and B)ONOO- levels in LPS/IFNγ-treated BMDMs (LPS 100 ng/ml + IFN-γ 20 ng/ml) incubated with PCOD585, PCOD@PLGA, M/PCOD@PLGA at dosage of 1 μM PCOD585. Scale bar: 50 μm. (n = 3–4). C) CLSM imaging and D) $ONOO^-$ levels in H/R-treated AMCMs (hypoxia:1 h/reoxygenation: 4 h) incubated with PCOD585, PCOD@PLGA, M/PCOD@PLGA at dosage of 1 μM PCOD585. Scale bar: 20 μm. (n = 5–6). E) TUNEL images and F) apoptosis levels in H/R-treated AMCMs incubated with PCOD585, PCOD@PLGA, M/PCOD@PLGA at equivalent dosage of 1μM PCOD585. Scale bar: 200 μm. (n = 4–6). G) Quantitation of CCK8 measurement of H/R-treated AMCMs incubated with PCOD585, PCOD@PLGA, M/PCOD@PLGA at equivalent dosage of 1μM PCOD585. (n = 10). H) Inflammatory gene expression of LPS/IFN-γ-treated BMDMs incubated with PCOD585, PCOD@PLGA, M/PCOD@PLGA at equivalent dosage of 1μM PCOD585. (n = 6). (NS no significance, *: $p < 0.05$, **: $p < 0.01$, ***: $p < 0.001$).

mimic the role of macrophage in MI/R injury [30]. Cardiomyocytes and macrophages generate $ONOO^-$ during MI/R injury [31,32]. Then, the ability of M/PCOD@PLGA to clear $ONOO^-$ in LPS/IFN-γ-treated BMDMs and H/R-treated AMCMs was evaluated in vitro. As expected, LPS/IFN-γ significantly induced $ONOO^-$ generation in BMDMs (Fig. 2A and B). However, when the BMDMs were cocultured with PCOD585, PCOD@PLGA, or M/PCOD@PLGA, the $ONOO^-$ levels decreased, but the most significant reduction was observed in the M/PCOD@PLGA group. Likewise, a similar effect was observed in AMCMs. H/R induced $ONOO^-$ generation in the AMCMs. PCOD585, PCOD@PLGA, and M/PCOD@PLGA treatment could reduce the $ONOO^-$ levels. Additionally, the most significant reduction in $ONOO^-$ levels was observed in the M/PCOD@PLGA group (Fig. 2C and D).

To further explore the protective effects of M/PCOD@PLGA, AMCM apoptosis was detected by TUNEL staining, and cell viability was measured by CCK8. H/R increased the number of TUNEL-positive AMCMs, which means H/R successfully induce AMCMs apoptosis. This increased level of apoptosis was ameliorated by PCOD585, PCOD@PLGA, and M/PCOD@PLGA treatment (Fig. 2E and F). Furthermore, CCK8 result revealed that all three treatments improved AMCM viability (Fig. 2G). However, the most significant of these effects were observed with M/PCOD@PLGA treatment.

The anti-inflammatory effects of M/PCOD@PLGA were next explored. The gene expression levels of M1 macrophage polarization markers were measured by RT-qPCR. PCOD585, PCOD@PLGA, and M/PCOD@PLGA treatment all significantly reduced the mRNA levels of interleukin 6 (*Il-6*), interleukin 1 beta (*Il-1β*), and tumor necrosis factor alpha (*Tnf-α*). However, M/PCOD@PLGA treatment more effectively inhibited the expression of these M1 macrophage polarization markers in vitro compared with the other two treatments (Fig. 2H). Previous study proved that the nanoparticles coated with macrophage membrane could absorb endotoxins and proinflammatory cytokines, since the cytokine binding receptors on macrophage membrane have high affinity to LPS and cytokines [33]. We further explore the cytokines-neutralization ability of M/PCOD@PLGA. LPS, IL6, TNF-α and IFN-γ were respectively mixed with PCOD@PLGA or M/PCOD@PLGA for indicated time and the concentration of cytokines were quantified. The M/PCOD@PLGA could decrease LPS, IL6, TNF-α and IFN-γ, while PCOD@PLGA show no effects (Fig. S5). The cytokine absorbing effect of M/PCOD@PLGA could explain why M/PCOD@PLGA have better in vitro anti-inflammatory ability than both PCOD585 and PCOD@PLGA.

3.3. Cellular uptake of M/PCOD@PLGA in vitro

Previous study proved that the uptake of nanoparticles by the mononuclear phagocyte system (MPS) inhibits nanoparticle accumulation at the myocardial injury site [34]. Therefore, the immune escape ability of M/PCOD@PLGA was evaluated using fluorescently labeled nanoparticles (Cy5.5@PLGA and M/Cy5.5@PLGA). Compared with BMDMs cultured with Cy5.5@PLGA, BMDMs cultured with M/Cy5.5@PLGA group exhibited a lower fluorescence signal, which indicated that the macrophage membrane-coated nanoparticles escaped

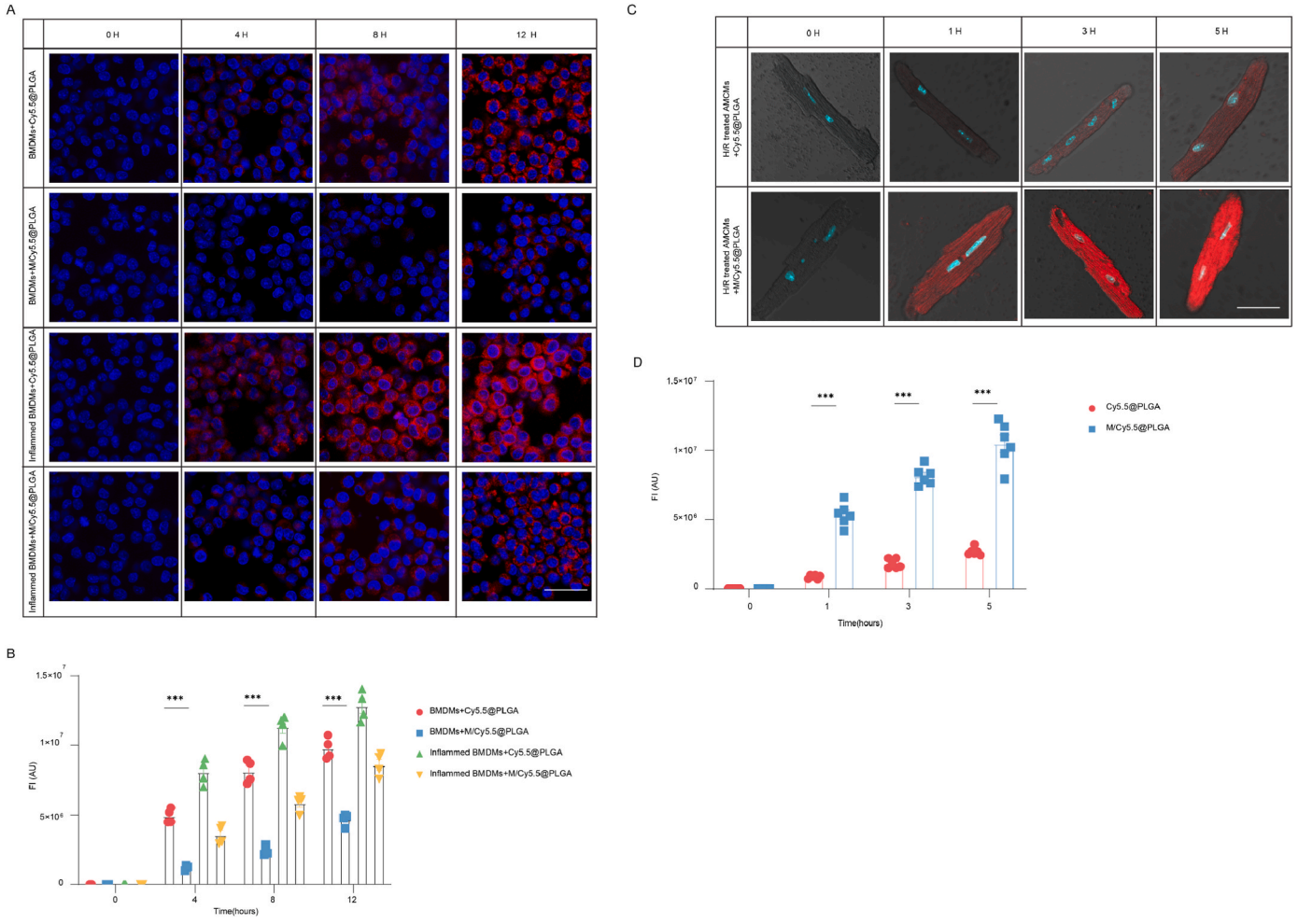

Fig. 3. In vitro cellular uptake of nanoparticles
A, C) CLSM images and B, D) quantitative analysis of cellular uptake of Cy5.5@PLGA and M/Cy5.5@PLGA by non-inflamed BMDMs and inflamed BMDMs (LPS 100 ng/ml + IFNγ 20 ng/ml) (n = 4) H/R treated AMCMs (n = 6). Scale bar: 50 μm **: $p < 0.01$, ***: $p < 0.001$.

from uptake by the cells. Furthermore, stronger fluorescence was detected in BMDMs cultured with M/Cy5.5@PLGA after the cells were treated with LPS/IFN-γ to induce inflammation. This indicated that the inflammation promoted the uptake of M/Cy5.5@PLGA by the BMDMs (Fig. 3A and B), which was consistent with previous research [35]. Compared with PCOD@PLGA, cellular uptake of M/PCOD@PLGA in inflamed BMDMs is only improved in a less extent. This phenomenon was probably due to immune-evasive properties of macrophage membrane and negative potential of the particles on macrophage membrane [36]. Compared with unmodified PLGA, macrophage membrane coated nanoparticles have enhanced ability to evade phagocytosis by MPS, resulting in longer blood-circulation time [37]. Then, the in vivo pharmacokinetics of PCOD@PLGA and M/PCOD@PLGA nanoparticles were evaluated. As shown in Fig. S6, M/Cy5.5@PLGA had longer blood circulation time, due to the coated macrophage membrane.

The effects of the macrophage membrane coating on the uptake efficiency of nanoparticles were further investigated in AMCMs. H/R treated AMCMs were incubated with Cy5.5@PLGA or M/Cy5.5@PLGA with equivalent concentrations of Cy5.5. The uptake of M/Cy5.5@PLGA by the AMCMs was significantly higher than that of Cy5.5@PLGA (Fig. 3C and D). The increased uptake of M/Cy5.5@PLGA by AMCMs was probably due to vascular cell adhesion molecule (VCAM) expressed on H/R-treated AMCMs (Fig. S7A). VCAM could interact with integrin α4β1 receptor expression on the macrophage membrane, which enhance the adhesion and uptake of M/Cy5.5@PLGA on AMCMs. To evaluate this possibility, the integrin α4β1 on M/Cy5.5@PLGA was blocked by antibodies. Compared with M/Cy5.5@PLGA, M/Cy5.5@PLGA(blocked) showed lower cellular uptake levels in H/R treated AMCMs (Fig. S7B).

3.4. Targeted delivery of M/PCOD@PLGA in a MI/R mice

To further explore the targeting capability of M/PCOD@PLGA to the MI/R injury site, the myocardial distribution of the nanoparticles was evaluated in a mouse model of MI/R injury. The mice were injected with Cy5.5@PLGA or M/Cy5.5@PLGA via the tail vein, and fluorescence was detected 6 h later. A stronger fluorescence signal was detected in the myocardial tissues of the M/Cy5.5@PLGA-treated group compared with that of the Cy5.5@PLGA-treated group (Fig. 4E and F). Fluorescence was also evaluated in other major organs, but there was no difference in the distribution of the nanoparticles (Figs. S8A and B). This indicated that the coated macrophage membrane did not influence the distribution of the nanoparticles in other organs. These results demonstrated that more nanoparticles accumulated in the myocardial tissues of the M/Cy5.5@PLGA-treated group than those of the Cy5.5@PLGA-treated group (Fig. 4A and B). MI/R injury induces VCAM expression in cardiomyocytes, which enhance the adhesion of nanoparticles in the ischemic area [38]. Significant colocalization was observed between the nanoparticles and VCAM in the M/Cy5.5@PLGA-treated group (Fig. 4C

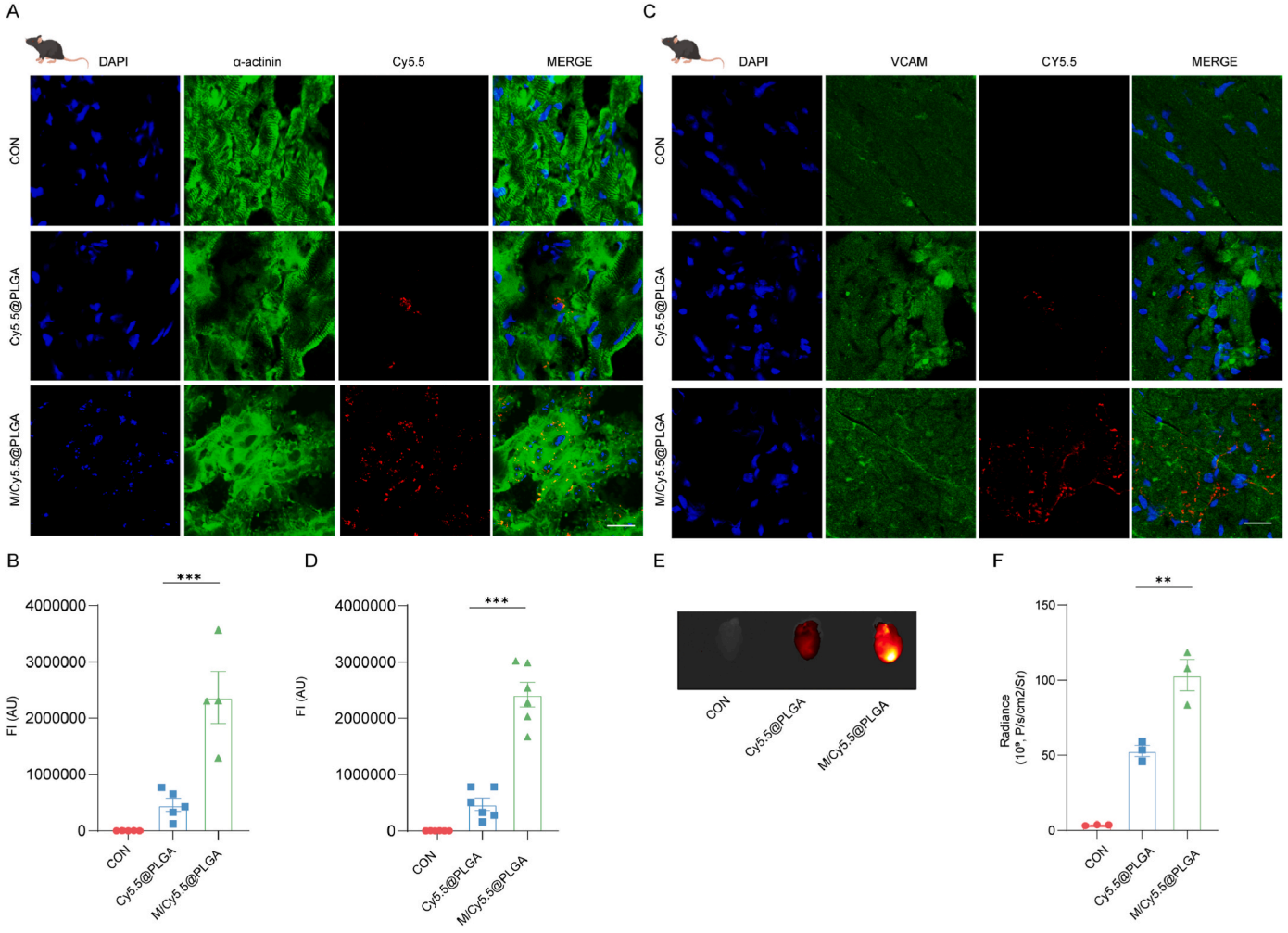

Fig. 4. In vivo targeting ability of M/PCOD@PLGA.
A, C) CLSM images and B, D)fluorescence signals accumulated in the hearts section staining with A, B) α-actinin (n = 4–5) C, D) VCAM (n = 6) from MI/R mice after injection of Cy5.5(CON), Cy5.5@PLGA, M/Cy5.5@PLGA. Scale bar: 20 μm. E) IVIS images and F) fluorescence signals accumulated in the hearts from MI/R mice. (n = 3). **: $p < 0.01$, ***: $p < 0.001$.

and D). Altogether, these results indicated that the macrophage membrane-coated nanoparticles exhibited enhanced targeting efficiency to the myocardial ischemic area in vivo.

3.5. M/PCOD@PLGA ameliorated MI/R injury

The therapeutic efficacy of PCOD585, PCOD@PLGA, and M/PCOD@PLGA against MI/R injury was next explored. Echocardiography was utilized to analyze the early cardiac function of mice one day after MI/R injury (Fig. 5A). Compared to the sham group, the MI/R group showed a significant reduction in both ejection fraction (EF) and fractional shortening (FS), indicating a decline in cardiac function. M/PCOD@PLGA (at a dose of 6 mg/kg PCOD585) treatment increased both EF and FS, whereas PCOD585 (6 mg/kg) or PCOD@PLGA (at a dose of 6 mg/kg PCOD585) treatment did not have any positive effect on these parameters (Fig. 5B and C). TTC staining revealed that M/PCOD@PLGA treatment also reduced infarction size, but the other treatments did not have this effect (Fig. 5 J, K, L). We further evaluated the late outcomes of MI/R mice received different treatment. Sirius Red and Masson staining of mouse myocardial tissues revealed that M/PCOD@PLGA treatment successfully decreased myocardial fibrosis and collagen deposition 14 days after MI/R injury (Figs. S9A, B, C, D). Additionally, the mice of the M/PCOD@PLGA treatment group exhibited a higher EF and FS than the mice of the MI/R group (Figs. S9E, F, G). Moreover, M/PCOD@PLGA treatment improved the overall left ventricular end-diastolic volume (LVEDV) and left ventricular end-systolic volume (LVESV) of mice after MI/R injury, indicating that the treatment attenuated left ventricular enlargement due to MI/R injury (Figs. S9H and I).

Apoptosis serves as key mechanism in MI/R injury [39]. Thus, the expression of apoptosis-related proteins was next evaluated. Compared with MI/R mice who did not receive the treatment, MI/R mice with M/PCOD@PLGA treatment showed a decrease in the expression of

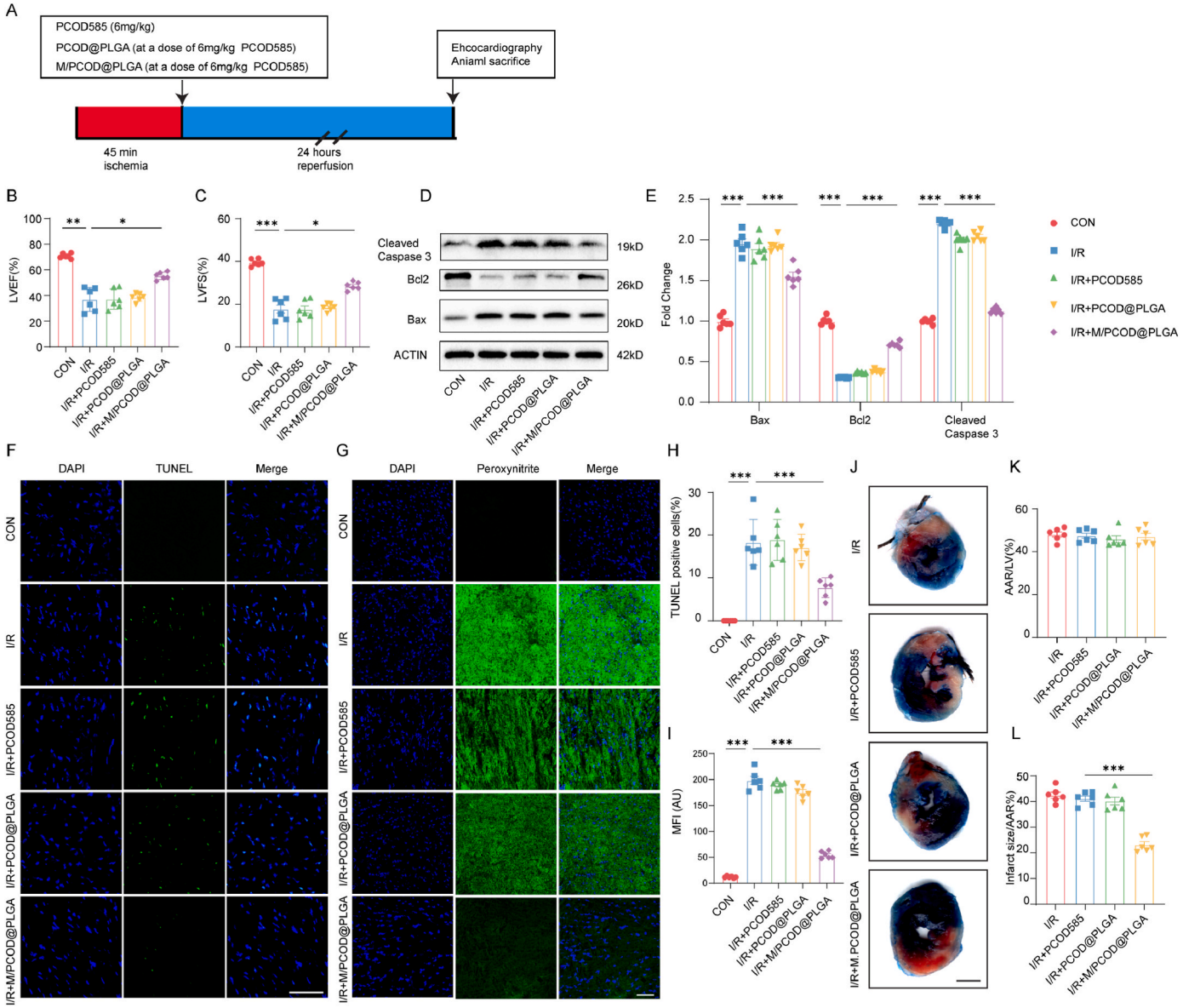

Fig. 5. Therapeutic effect of M/PCOD@PLGA in MI/R model following i. v. administration
A) The experimental scheme of the mice with acute I/R injury treated with different formulas of PCOD585 B, C) Left ventricular ejection fractions (EF) and left ventricular fractional shortening (FS) in at 1 day post-MI/R mice. D, E) Bax, Bcl-2, and cleaved caspase 3 expressions in ischemic heart tissues of mice at 1 day post-MI/R. F) CLSM image and H) quantitative analysis of TUNEL staining of ischemic heart area of mice at 1 day post-MI/R. Scale bar: 50 μm. G) CLSM image and I) quantitative analysis of $ONOO^-$ staining of mice ischemic heart area at 1 day post-MI/R. Scale bar: 50 μm. J, K, L) left ventricular (LV) tissue sections stained with Evans blue and TTC at 1 day post-MI/R to define the area at risk (AAR) and the infarcted regions. Scale bar: 1 mm ***: $p < 0.001$. (n = 6).

pro-apoptotic proteins, such as cleaved caspase-3 and BAX, while the expression of the anti-apoptotic protein BCL-2 increased (Fig. 5D and E). TUNEL staining further revealed that apoptosis was decreased in the myocardial tissues of the M/PCOD@PLGA-treated mice after MI/R injury, whereas this effect was not observed in the tissues from the mice of the PCOD585 and PCOD@PLGA treatment groups (Fig. 5F, H).

Next, the $ONOO^-$-scavenging ability of the three treatments were evaluated in vivo. Immunofluorescence analysis demonstrated that M/PCOD@PLGA treatment significantly reduced the accumulation of $ONOO^-$ (Fig. 5G, I). Western blot analysis revealed that levels of the protein S-nitrosylation were consistent with these results. Specifically, M/PCOD@PLGA treatment decreased the levels of total protein S-nitrosylation induced by MI/R injury (Figs. S10A and B).

To further verify the anti-inflammatory effects of M/PCOD@PLGA, the mRNA levels of M1 (*Il-1β*, *Il-6*, and *Tnf-α*) and M2 macrophage polarization markers (interleukin 10 [*Il-10*] and arginase-1[*Arg-1*]) were evaluated in ischemic myocardial tissues. Compared with the control group, MI/R injury increased the expression of *Il-1β*, *Il-6*, and *Tnf-α* and decreased the expression of *Il-10* and *Arg-1*. In contrast, M/PCOD@PLGA treatment reduced this elevated expression of the M1 macrophage polarization markers and increased the reduced expression of the M2 macrophage polarization markers after MI/R, but these effects were not observed with PCOD585 or PCOD@PLGA treatment (Fig. 6A, B, C, D, E). Next, flow cytometry was used to further evaluate macrophage polarization in the myocardial tissues of the mice after MI/R, according to the gating strategy shown in Fig. S11. M/PCOD@PLGA decreased the number of pro-inflammatory (CD45 + CD11b + Ly6G-F4/80 + $Ly6C^{high}$) macrophages and increased that of anti-inflammatory (CD45 + CD11b + Ly6G-F4/80 + $Ly6C^{low}$) macrophages in the early phase after MI/R in the myocardial tissues of the mice (Fig. 6F, G, H). The scatter diagram was shown in Fig. S12. In summary, these results indicated that M/PCOD@PLGA treatment modulated the inflammatory response induced by MI/R injury.

Mitochondria serve as a vital intracellular organelle in cardiomyocytes that can be damaged by MI/R injury [14]. As previously reported, CO improves mitochondrial energy metabolism and enhances mitochondrial biogenesis, thus suggesting it as a potential therapeutic agent [19,40]. A Seahorse analyzer was used to measure the mitochondrial respiratory capacity of AMCMs isolated from mice after MI/R injury and administration of one of the three treatments. M/PCOD@PLGA treatment significantly increased ATP production as well as the basal and maximum respiration of AMCMs compared with those of the MI/R group (Fig. 7A, B, C, D). M/PCOD@PLGA treatment also ameliorated the decreased ATP content induced by MI/R injury

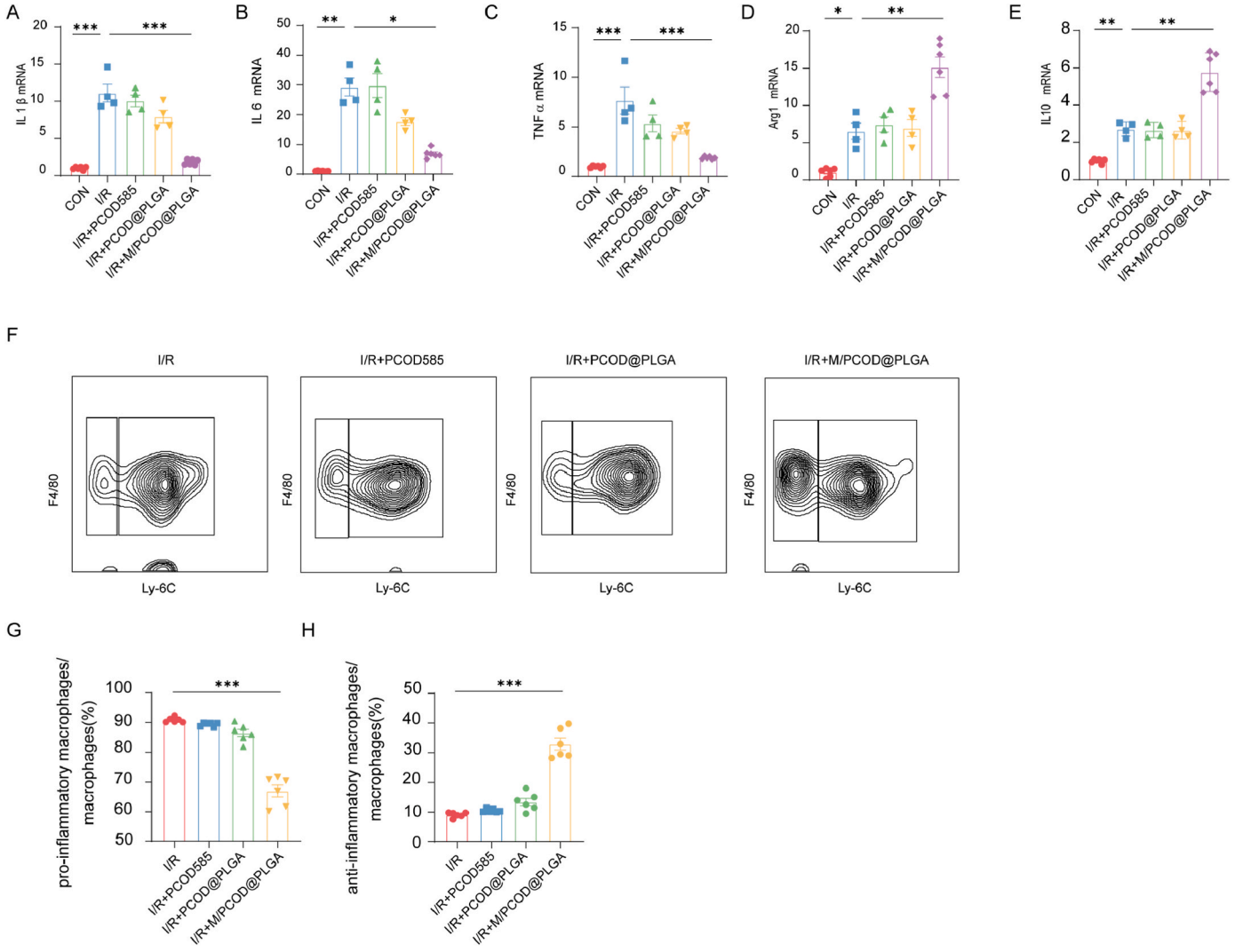

Fig. 6. M/PCOD@PLGA modulate inflammation in MI/R mice
A, B, C, D, E) mRNA expression levels of IL-10, IL-1β, TNF-α, IL-6, and Arg1 in the ischemic heart area of mice at 1 day post-MI/R were examined by RT-qPCR. (n = 4–5). F) Representative images and G, H) quantitative analysis of flow cytometric analysis of infiltrated proinflammatory ($CD45^+CD11b^+Ly\text{-}6G^-F4/80^+Ly\text{-}6C^{high}$) and anti-inflammatory ($CD45^+$ $CD11b^+Ly\text{-}6G^-F4/80^+Ly\text{-}6C^{low}$) macrophages in LV of mice at 1 day post-MI/R. (n = 6). **: $p < 0.01$, ***: $p < 0.001$.

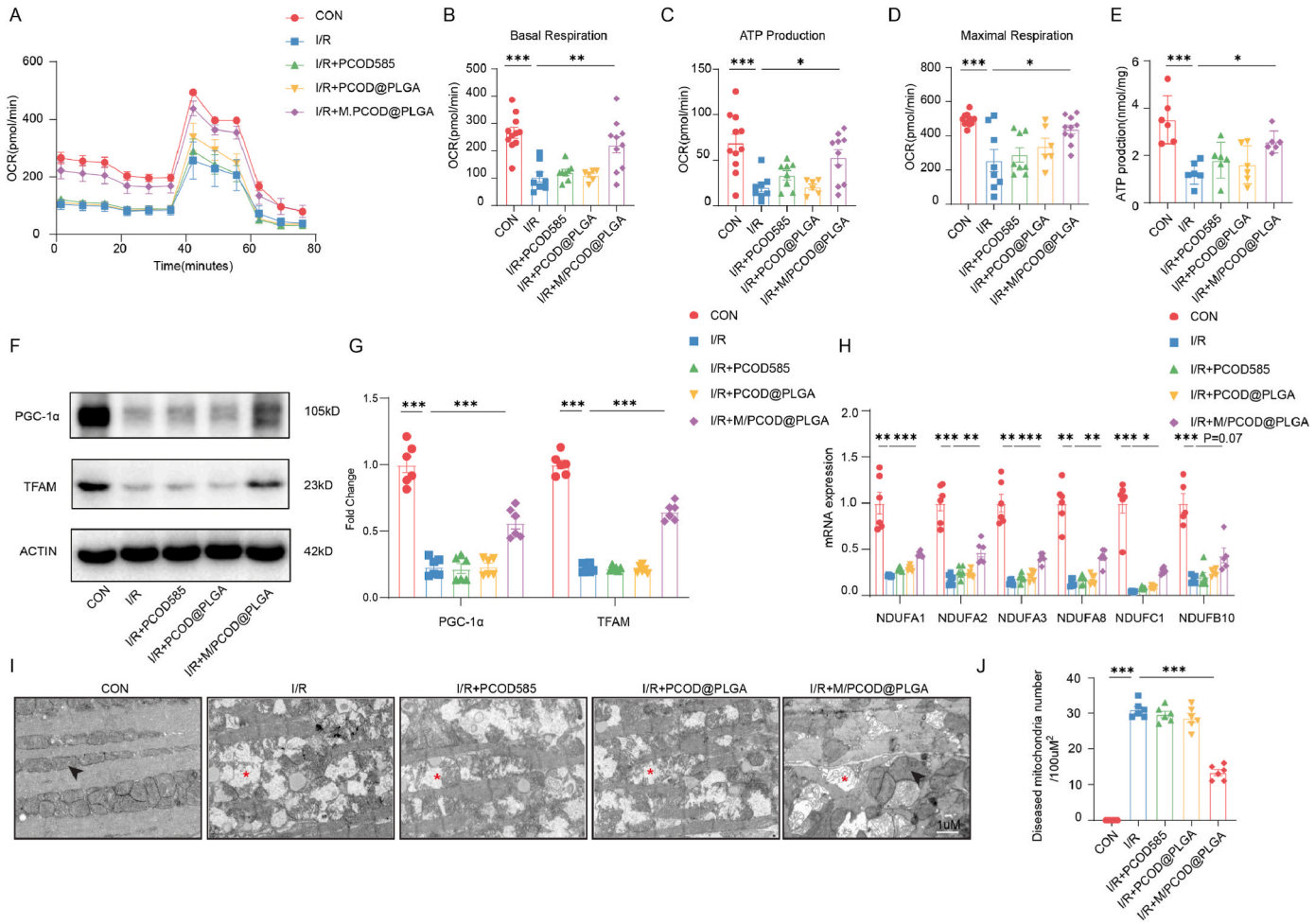

Fig. 7. M/PCOD@PLGA promotes mitochondria biogenesis and energy metabolism in vivo
A) Mitochondrial respiration measurement of AMCMs isolated from mice at 1 day post-MI/R. B, C, D) Basal respiration, ATP production, maximal respiration of AMCMs isolated from mice at 1 day post-MI/R. (n = 6–11). E) ATP production measurement of heart tissues from mice at 1 day post-MI/R. (n = 6). F, G) Protein expression of PGC1α and TFAM in ischemic heart tissues of mice at 1 day post-MI/R. (n = 6). H) Relative expression of mitochondrial respiratory complex genes in the heart from PCOD585, PCOD@PLGA, M/PCOD@PLGA treated mice at 1 day post-MI/R. (n = 4–6). I) Representative images of cardiac mitochondrial morphology by TEM (Red asterisk: diseased mitochondria, Black arrow: normal mitochondria). Scale bar: 1 μm. J) Diseased mitochondrial number. (n = 6). *: $p < 0.05$, **: $p < 0.01$, ***: $p < 0.001$.

(Fig. 7E). No significant differences were observed among the MI/R, PCOD, and PCOD@PLGA groups. The expression of key proteins in mitochondrial biogenesis, including peroxisome proliferator-activated receptor gamma coactivator 1-alpha (PGC1A) and mitochondrial transcription factor A (TFAM) were next examined to evaluate the ability of M/PCOD@PLGA to enhance mitochondrial biogenesis [41]. MI/R injury decreased the expression of PGC1A and TFAM compared with the control group. However, M/PCOD@PLGA treatment attenuated this decrease in PGC1A and TFAM expression after MI/R injury (Fig. 7F and G). Consistent with these results, the expression of the genes encoding these proteins of the mitochondrial respiratory complex was decreased after MI/R injury, whereas M/PCOD@PLGA treatment attenuated this decreased expression (Fig. 7H). Next, mitochondrial morphology was analyzed by TEM in the ischemic cardiac tissues. TEM revealed damaged mitochondria with swollen mitochondrial matrixes and disordered mitochondrial cristae. The MI/R injury led to an increase in the number of damaged mitochondria, whereas treatment with M/PCOD@PLGA significantly decreased the number of damaged mitochondria (Fig. 7I and J). These findings indicated that M/PCOD@PLGA treatment ameliorated mitochondrial dysfunction in cardiomyocytes after MI/R injury.

3.6. CO production in vivo

To compare the CO production effect of PCOD585 and M/PCOD@PLGA, we treat MI/R mice with different dose of PCOD585 (6 mg/kg, 15 mg/kg, 30 mg/kg). PCOD585 (30 mg/kg) treatment could improve EF and FS, which is similar to the effect of M/PCOD@PLGA (at a dose of 6 mg/kg PCOD585) treatment (Fig. S13). Then we detect the CO concentration of heart tissue from MI/R mice accept PCOD585 and M/PCOD@PLGA treatment. In PCOD585 (6 mg/kg) treatment group, the concentration of CO is 7.574 ± 0.9893 pmol/mg (3 h), 6.230 ± 0.6903 pmol/mg (6 h), 5.905 ± 0.5501 pmol/mg (24 h). In PCOD585 (15 mg/kg) treatment group, the concentration of CO is 12.44 ± 1.096 pmol/mg (3 h), 10.74 ± 0.8454 pmol/mg (6 h), 7.003 ± 0.5932 pmol/mg (24 h). In PCOD585 (30 mg/kg) treatment group, the concentration of CO is 22.40 ± 1.060 pmol/mg (3 h), 18.94 ± 1.378 pmol/mg (6 h), 8.613 ± 0.6355 pmol/mg (24 h). In M/PCOD@PLGA treatment group (at a dose of 6 mg/kg PCOD585), the concentration of CO is 24.05 ± 1.964 pmol/mg (3 h), 20.44 ± 1.098 pmol/mg (6 h), 9.399 ± 0.8809 pmol/mg (24 h) (Fig. S14).

3.7. Biosafety assessment of M/PCOD@PLGA in vivo

The biosafety of the treatments was next assessed in C57BL/6J mice. Hematoxylin and eosin (H&E) staining of the major organs (spleen, kidneys, liver, lungs, and brain) showed no obvious signs of damage after treatment injection (Fig. 8A). Blood gas analysis revealed that the carboxyhemoglobin concentrations were below toxic levels (Fig. 8B). Additionally, the treatments did not cause any significant alterations in the levels of biomarkers for liver function (alanine transaminase [ALT] and aspartate transaminase [AST]) and kidney function (creatine) in the mice (Fig. 8 C, D, E). Therefore, these results confirmed the biosafety of M/PCOD@PLGA.

4. Discussion

Here, we firstly confirmed that M/PCOD@PLGA could prevent MI/R induced cardiac dysfunction. The M/PCOD@PLGA consist of following three parts: PCOD585, PLGA and macrophage membrane. The mechanism of M/PCOD@PLGA was presented briefly as below. Because the coated macrophage membrane protect nanoparticle from clearance of MPS and could target inflammatory area, M/PCOD@PLGA could efficiently accumulated at ischemic area after being injected through tail vein. Integrin α4β1 expressed on coated macrophage membrane facilitated M/PCOD@PLGA adhere to the injured myocardium. And then, M/PCOD@PLGA would be internalized by nearby cells and released PCOD585 continuously. PCOD585 could react with intracellular ONOO- to generate CO locally. In this way, M/PCOD@PLGA achieved $ONOO^-$-triggered CO release in ischemic area, which could minimize potential toxicity and optimize the curative effect of CO (inhibiting excessive inflammation, alleviating apoptosis, mitigating mitochondrial dysfunction). In addition, cytokine receptors expressed on macrophage membrane enable M/PCOD@PLGA to absorb proinflammatory cytokines. By neutralizing these cytokines, M/PCOD@PLGA could further alleviate the excessive inflammation.

PLGA is an FDA-approved drug deliver carrier with good biocompatibility and biodegradability [42]. After being encapsulated into PLGA nanoparticles, the therapeutic agents are stable in nanoparticles and could be released sustainably [43]. However, the nonspecific clearance of nanoparticles by MPS would impair nanoparticles ability to accumulate in disease area [34]. To overcome this shortage, we developed a

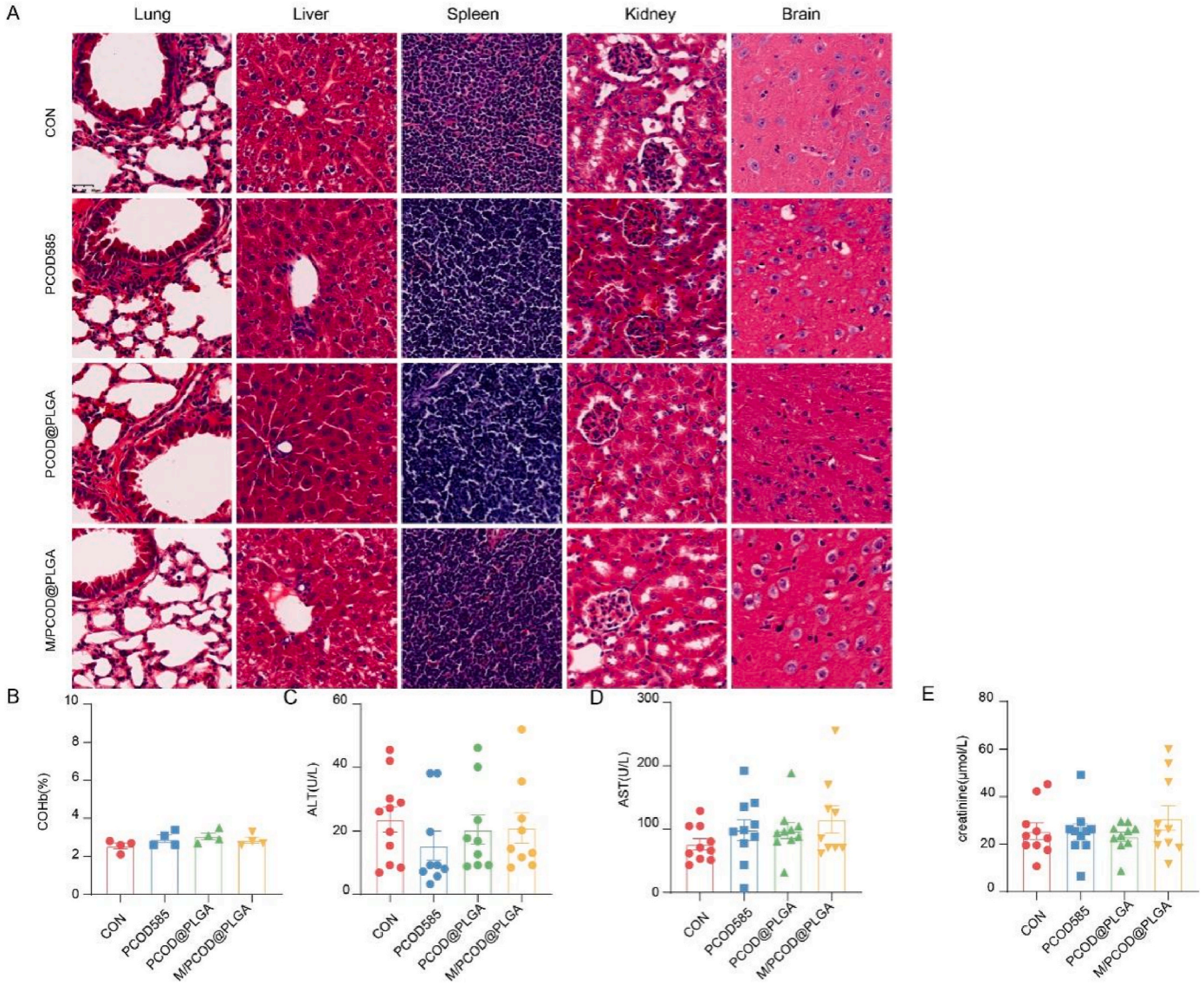

Fig. 8. Biosafety of M/PCOD@PLGA in vivo.
A) HE staining of major organs after indicated treatments. bar = 50 μm. B) COHb percentages in mice after indicated treatments. (n = 4). C, D, E) Quantitative analysis of AST, ALT, creatinine after indicated treatments. (n = 9–11).

biomimetic nanoplatform by coating macrophage membrane on PLGA. Our in vitro cellular uptake experiment proved that macrophage membrane-coating would significantly help nanoparticles escape from the internalization of nanoparticles by macrophage. By this way, membrane coated nanoparticles have longer circulation time in vivo. Obviously, the ability of macrophage membrane coating to prevent nanoparticles from clearance by MPS was verified in our experiment, which in line with other studies [43–45]. This ability to escape from the MPS clearance is related with the CD47 proteins expressed on macrophage membrane [46], which could also be observed on M/PCOD@PLGA in our study. Another advantage of coating macrophage membrane on nanoparticles is that macrophage membrane coated nanoparticles could target to inflamed area and adhere to injured cardiomyocytes, which enhance cardiomyocytes cell uptake of nanoparticles. The C–C chemokine ligand 2 (CCL2) bind with chemokine receptors (such as CCR2) expressed on macrophage membrane would help the recruitment of macrophage to inflamed tissues [47]. During MI/R injury, the ischemic area was found to secrete CCL2, which facilitated the recruitment of CCR2-positive macrophage [48]. Thus, we suggested that macrophage membrane coated nanoparticles could target to ischemic area by CCL2–CCR2 axis. Moreover, our data confirmed that the expression of adhesion molecules (VCAM-1) on cardiomyocyte can be induced by H/R injury, which is consistent with findings of other studies [38,49]. Then, the integrin α4β1 on macrophage membrane could bind with adhesion molecules on cardiomyocytes, which helps the accumulation of nanoparticles in ischemic area [49,50]. The presence of these molecules (CD47, CCR2, integrin α4β1) on M/PCOD@PLGA were all verified by our experiments. Based on advantages above, we utilized macrophage membrane coated PLGA to deliver PCOD585. The in vivo target experiment proved that macrophage membrane coating enhanced the accumulation and adherence of M/PCOD@PLGA to injured myocardium and thereby achieved more efficient delivery of drug. Taken together, our results revealed that macrophage membrane coated nanoparticle could effectively deliver therapeutic agents to ischemic heart tissue in MI/R injury.

PCOD585 is a $ONOO^-$-responsive CO donor. Depending on this property, PCOD585 could eliminate $ONOO^-$ and generate CO subsequently. $ONOO^-$, derived from the reaction of nitric oxide and superoxide, serves as one of the main free radicals that cause cardiac dysfunction during MI/R injury [51]. Previous studies demonstrate that cardiomyocytes and macrophages would generate lots of ONOO- during MI/R injury [31,32]. Decreasing levels of $ONOO^-$ could alleviate MI/R injury [3,51,52]. In our study, the $ONOO^-$ clearance ability of M/PCOD@PLGA was verified both in vivo and in vitro. CO, produced from reaction between PCOD585 and $ONOO^-$, could inhibit cardiomyocyte apoptosis, suppress excessive inflammation and promote mitochondria biogenesis [18]. The therapeutic effect of the CO donor in ischemic heart disease have already been verified [53,54]. However, since uncontrollable diffusion and inefficient cellular uptake, high doses of CO donors were usually required to reach an effective CO concentration in diseased tissues [20]. M/PCOD@PLGA achieved precise delivery and controllable release of CO in the ischemia area, which ensure best therapeutic effect of M/PCOD@PLGA at a relatively low dose of PCOD585.

Excessive inflammation would aggravate cardiac dysfunction caused by MI/R injury [11,13]. The anti-inflammatory ability of nanoparticles was evaluated both in vitro and in vivo. Interestingly, we observed that M/PCOD@PLGA treatment have best anti-inflammatory ability in LPS/IFN-γ treated BMDMs in vitro, although LPS/IFN-γ treated BMDMs uptake less macrophage membrane coated nanoparticles. A series of studies also showed that membrane coated nanoparticles could have better anti-inflammatory ability than free drug and naked nanoparticles in vitro, although less drug have been internalized by macrophage [46,51]. The specific mechanism is that the cytokine receptors (such as TNFR, IL6R) on macrophage membrane could bind with proinflammatory cytokines and subsequently neutralize these cytokines [33,44,55]. This property could partially explain why M/PCOD@PLGA have best anti-inflammatory ability in vitro and in vivo. As for in vivo experiment, M/PCOD@PLGA treatment significantly decreased the mRNA levels of M1 marker (Il-1β, Il-6, and TNF-α) and increased the mRNA levels of M2 marker (IL-10 and Arg-1), which in consistent with results of flow cytometry. These results suggested that M/PCOD@PLGA have significant anti-inflammatory ability in vivo, which is partly due to targeting ability of M/PCOD@PLGA. The targeting ability ensure effective concentration of CO in ischemic area, which could inhibit inflammation [18].

Previous studies have confirmed that mitochondria dysfunction serves as key factor in MI/R injury [15]. It has been reported that CO could prevent mitochondrial dysfunction caused by doxorubicin through promoting mitochondrial biogenesis [40]. Seahorse experiment revealed M/PCOD@PLGA treatment significantly increased basal respiration, ATP production and maximal respiration of cardiomyocytes compared with MI/R group, which suggested that M/PCOD@PLGA treatment could protect mitochondrial oxidative phosphorylation function impairment caused by MI/R injury. Meanwhile, M/PCOD@PLGA treatment could enhance mitochondrial biogenesis through increasing expression of mitochondrial biogenesis key factors (PGC1A and TFAM). TEM also revealed that M/PCOD@PLGA treatment decrease number of diseased mitochondria, which in line with our seahorse results. Thus, we concluded that M/PCOD@PLGA could alleviate mitochondrial dysfunction caused by MI/R injury. We suggested that the therapeutic effects of M/PCOD@PLGA on mitochondrial function may be attributed to two aspects. Firstly, M/PCOD@PLGA could ensure a persistent higher concentration of CO in heart, which could ensure the protective effect of CO on mitochondria. Secondly, M/PCOD@PLGA treatment have better anti-inflammatory properties and $ONOO^-$-scavenging ability. Inflammatory cytokines and ROS generated during MI/R injury have been reported to impair mitochondrial function [56]. Thus, M/PCOD@PLGA could protect mitochondria by decreasing these harmful cytokines and $ONOO^-$. Taken together, M/PCOD@PLGA protect mitochondrial dysfunction by synergistic mechanism.

In general, the macrophage membrane enables M/PCOD@PLGA accumulated in ischemic area and M/PCOD@PLGA could neutralize proinflammatory cytokines, eliminate $ONOO^-$ and achieve controllable release of protective CO in ischemic area. Both in vivo and in vitro results indicated that M/PCOD@PLGA is a promising treatment for MI/R injury. Additionally, M/PCOD@PLGA also have good biosafety in vivo. There are still some limitations in our study. Firstly, we reported that M/PCOD@PLGA could alleviate MI/R injury through following mechanisms: clearing $ONOO^-$, inhibiting excessive inflammation and alleviate mitochondrial disorder. However, the mechanism of MI/R injury is complex and dynamic [14]. The most predominant mechanism that M/PCOD@PLGA exerts its protective function needs further exploration. Secondly, we treated MI/R mice with M/PCOD@PLGA at the beginning of reperfusion period, since drugs against MI/R injury usually be given to patients instantly after the PCI therapy. However, this might not be the best administration timepoint to maximize the therapeutic effect of M/PCOD@PLGA. The optimal schedule to give M/PCOD@PLGA still needs further study. Thirdly, co-extrusion method is a widely used, simple and mature method to produce cell membrane-coated nanoparticles, which is usually used in basic research. However, it is difficult to prepare cell membrane-coated nanoparticles on a large scale by co-extrusion method, which limited potential clinical translation of M/PCOD@PLGA. Thus, the methodology to produce M/PCOD@PLGA through some advanced technology (such as microfluidic electroporation method) need further study.

5. Conclusions

In this study, a biomimetic, macrophage-like nanoparticle delivery system, M/PCOD@PLGA, has been generated to treat MI/R injury. This biomimetic, PLGA-based, $ONOO^-$-responsive CO nanogenerator

exhibits several features: 1) the targeted delivery of nanoparticles to the site of MI/R injury, 2) the ability to precisely scavenge $ONOO^-$ in a timely manner, and 3) the controlled and continuous release of CO as a product of the reaction between PCOD585 and $ONOO^-$ in the ischemic area. The conceptual design of M/PCOD@PLGA undoubtedly offers a more precise, sensitive, and safer alternative for the targeted and controlled administration of CO and thus addresses the existing challenges of treatment with CO gas.

CRediT authorship contribution statement

Jinyan Zhang: Methodology, Validation, Formal analysis, Data curation, Conceptualization, Investigation, Writing – review & editing. **Liwei Liu:** Methodology, Data curation. **Zhen Dong:** Methodology, Conceptualization, Writing – review & editing. **Xicun Lu:** Methodology. **Wenxuan Hong:** Methodology. **Jin Liu:** Methodology. **Xiaoyi Zou:** Methodology. **Jinfeng Gao:** Methodology. **Hao Jiang:** Methodology. **Xiaolei Sun:** Methodology, Writing – review & editing. **Kai Hu:** Writing – review & editing. **Youjun Yang:** Conceptualization, Writing – review & editing. **Junbo Ge:** Conceptualization, Funding acquisition. **Xiao Luo:** Supervision, Conceptualization, Investigation. **Aijun Sun:** Supervision, Funding acquisition, Conceptualization, Investigation, Writing – review & editing.

Declaration of competing interest

The authors declare that they have no known competing financial interests or personal relationships that could have appeared to influence the work reported in this paper.

Acknowledgements

The authors acknowledge the support by the National Natural Science Foundation of China (81900353, 82270264, T2288101, 82130010, 21908065, 22078098, 22278138), the National Science Fund for Distinguished Young Scholars (817200010), the Basic research projects of Shanghai Science and Technology Commission (22JC1400500) and the Innovation Program of Shanghai Municipal Education Commission.

Appendix A. Supplementary data

Supplementary data to this article can be found online at https://doi.org/10.1016/j.bioactmat.2023.05.017.

References

[1] D. Hausenloy, D. Yellon, Ischaemic conditioning and reperfusion injury, Nat. Rev. Cardiol. 134 (2016) 193–209, https://doi.org/10.1038/nrcardio.2016.5.
[2] D. Yellon, D. Hausenloy, Myocardial reperfusion injury, N. Engl. J. Med. 35711 (2007) 1121–1135, https://doi.org/10.1056/NEJMra071667.
[3] Y. Zhang, J. Bissing, L. Xu, Nitric oxide synthase inhibitors decrease coronary sinus-free radical concentration and ameliorate myocardial stunning in an ischemia-reperfusion model, J. Am. Coll. Cardiol. 382 (2001) 546–554, https://doi.org/10.1016/s0735-1097(01)01400-0.
[4] J. Beckman, W. Koppenol, Nitric oxide, superoxide, and peroxynitrite: the good, the bad, and ugly, Am. J. Physiol. 271 (1996) C1424–C1437, https://doi.org/10.1152/ajpcell.1996.271.5.C1424.
[5] Y. Hayashi, Y. Sawa, S. Ohtake, Peroxynitrite formation from human myocardium after ischemia-reperfusion during open heart operation, Ann. Thorac. Surg. 722 (2001) 571–576, https://doi.org/10.1016/s0003-4975(01)02668-6.
[6] S. Korkmaz, T. Radovits, E. Barnucz, Pharmacological activation of soluble guanylate cyclase protects the heart against ischemic injury, Circulation 1208 (2009) 677–686, https://doi.org/10.1161/circulationaha.109.870774.
[7] A.J. Lokuta, N.A. Maertz, S.V. Meethal, Increased nitration of sarcoplasmic reticulum Ca2+-ATPase in human heart failure, Circulation 1118 (2005) 988–995, https://doi.org/10.1161/01.Cir.0000156461.81529.D7.
[8] A.C. Montezano, R.M. Touyz, Reactive oxygen species and endothelial function–role of nitric oxide synthase uncoupling and Nox family nicotinamide adenine dinucleotide phosphate oxidases, Basic Clin. Pharmacol. Toxicol. 1101 (2012) 87–94, https://doi.org/10.1111/j.1742-7843.2011.00785.x.
[9] J. Xu, M.H. Zou, Molecular insights and therapeutic targets for diabetic endothelial dysfunction, Circulation 12013 (2009) 1266–1286, https://doi.org/10.1161/circulationaha.108.835223.
[10] F. Montecucco, F. Carbone, T.H. Schindler, Pathophysiology of ST-segment elevation myocardial infarction: novel mechanisms and treatments, Eur. Heart J. 3716 (2016) 1268–1283, https://doi.org/10.1093/eurheartj/ehv592.
[11] Q. Fan, R. Tao, H. Zhang, Dectin-1 contributes to myocardial ischemia/reperfusion injury by regulating macrophage polarization and neutrophil infiltration, Circulation 1395 (2019) 663–678, https://doi.org/10.1161/CIRCULATIONAHA.118.036044.
[12] R. Hinkel, P. Lange, B. Petersen, Heme oxygenase-1 gene therapy provides cardioprotection via control of post-ischemic inflammation: an experimental study in a pre-clinical pig model, J. Am. Coll. Cardiol. 662 (2015) 154–165, https://doi.org/10.1016/j.jacc.2015.04.064.
[13] M. DeBerge, X.Y. Yeap, S. Dehn, MerTK cleavage on resident cardiac macrophages compromises repair after myocardial ischemia reperfusion injury, Circ. Res. 1218 (2017) 930–940, https://doi.org/10.1161/circresaha.117.311327.
[14] Y. Li, B. Chen, X. Yang, S100a8/a9 signaling causes mitochondrial dysfunction and cardiomyocyte death in response to ischemic/reperfusion injury, Circulation 1409 (2019) 751–764, https://doi.org/10.1161/CIRCULATIONAHA.118.039262.
[15] G. Paradies, G. Petrosillo, M. Pistolese, Decrease in mitochondrial complex I activity in ischemic/reperfused rat heart: involvement of reactive oxygen species and cardiolipin, Circ. Res. 941 (2004) 53–59, https://doi.org/10.1161/01.Res.0000109416.56608.64.
[16] H.P. Indo, H.C. Yen, I. Nakanishi, A mitochondrial superoxide theory for oxidative stress diseases and aging, J. Clin. Biochem. Nutr. 561 (2015) 1–7, https://doi.org/10.3164/jcbn.14-42.
[17] M. Liesa, I. Luptak, F. Qin, Mitochondrial transporter ATP binding cassette mitochondrial erythroid is a novel gene required for cardiac recovery after ischemia/reperfusion, Circulation 1247 (2011) 806–813, https://doi.org/10.1161/circulationaha.110.003418.
[18] R. Motterlini, L. Otterbein, The therapeutic potential of carbon monoxide, Nat. Rev. Drug Discov. 99 (2010) 728–743, https://doi.org/10.1038/nrd3228.
[19] N.C. MacGarvey, H.B. Suliman, R.R. Bartz, Activation of mitochondrial biogenesis by heme oxygenase-1-mediated NF-E2-related factor-2 induction rescues mice from lethal Staphylococcus aureus sepsis, Am. J. Respir. Crit. Care Med. 1858 (2012) 851–861, https://doi.org/10.1164/rccm.201106-1152OC.
[20] H. Yan, J. Du, S. Zhu, Emerging delivery strategies of carbon monoxide for therapeutic applications: from CO gas to CO releasing nanomaterials, Small Methods 1549 (2019), e1904382, https://doi.org/10.1002/smll.201904382.
[21] J. Cheng, B. Zheng, S. Cheng, Metal-free carbon monoxide-releasing micelles undergo tandem photochemical reactions for cutaneous wound healing, Chem. Sci. 1117 (2020) 4499–4507, https://doi.org/10.1039/d0sc00135j.
[22] J.D. Byrne, D. Gallo, H. Boyce, Delivery of therapeutic carbon monoxide by gas-entrapping materials, Sci. Transl. Med. 14651 (2022), eabl4135, https://doi.org/10.1126/scitranslmed.abl4135.
[23] L. Xing, B. Wang, J. Li, A fluorogenic ONOO(-)-Triggered carbon monoxide donor for mitigating brain ischemic damage, J. Am. Chem. Soc. 1445 (2022) 2114–2119, https://doi.org/10.1021/jacs.2c00094.
[24] J. Zhuang, R.H. Fang, L. Zhang, Preparation of particulate polymeric therapeutics for medical applications, Small Methods 19 (2017), https://doi.org/10.1002/smtd.201700147.
[25] B.W. Michel, A.R. Lippert, C.J. Chang, A reaction-based fluorescent probe for selective imaging of carbon monoxide in living cells using a palladium-mediated carbonylation, J. Am. Chem. Soc. 13438 (2012) 15668–15671, https://doi.org/10.1021/ja307017b.
[26] M. Ackers-Johnson, P.Y. Li, A.P. Holmes, A simplified, langendorff-free method for concomitant isolation of viable cardiac myocytes and nonmyocytes from the adult mouse heart, Circ. Res. 1198 (2016) 909–920, https://doi.org/10.1161/CIRCRESAHA.116.309202.
[27] H.J. Vreman, R.J. Wong, T. Kadotani, Determination of carbon monoxide (CO) in rodent tissue: effect of heme administration and environmental CO exposure, Anal. Biochem. 3412 (2005) 280–289, https://doi.org/10.1016/j.ab.2005.03.019.
[28] J.A. Durlak, How to select, calculate, and interpret effect sizes, J. Pediatr. Psychol. 349 (2009) 917–928, https://doi.org/10.1093/jpepsy/jsp004.
[29] Y. Wang, K. Zhang, X. Qin, Biomimetic nanotherapies: red blood cell based core-shell structured nanocomplexes for atherosclerosis management, Adv. Sci. 612 (2019), 1900172, https://doi.org/10.1002/advs.201900172.
[30] H. Tan, Y. Song, J. Chen, Platelet-like fusogenic liposome-mediated targeting delivery of miR-21 improves myocardial remodeling by reprogramming macrophages post myocardial ischemia-reperfusion injury, Adv. Sci. 815 (2021), e2100787, https://doi.org/10.1002/advs.202100787.
[31] D. Polewicz, V. Cadete, A. Doroszko, Ischemia induced peroxynitrite dependent modifications of cardiomyocyte MLC1 increases its degradation by MMP-2 leading to contractile dysfunction, J. Cell Mol. Med. 155 (2011) 1136–1147, https://doi.org/10.1111/j.1582-4934.2010.01094.x.
[32] J. Kingery, T. Hamid, R. Lewis, Leukocyte iNOS is required for inflammation and pathological remodeling in ischemic heart failure, Basic Res. Cardiol. 1122 (2017) 19, https://doi.org/10.1007/s00395-017-0609-2.
[33] S. Thamphiwatana, P. Angsantikul, T. Escajadillo, Macrophage-like nanoparticles concurrently absorbing endotoxins and proinflammatory cytokines for sepsis management, in: Proceedings of the National Academy of Sciences of the United States of America, vol. 11443, 2017, pp. 11488–11493, https://doi.org/10.1073/pnas.1714267114.

[34] E. Blanco, H. Shen, M. Ferrari, Principles of nanoparticle design for overcoming biological barriers to drug delivery, Nat. Biotechnol. 339 (2015) 941–951, https://doi.org/10.1038/nbt.3330.
[35] C. Gao, Q. Huang, C. Liu, Treatment of atherosclerosis by macrophage-biomimetic nanoparticles via targeted pharmacotherapy and sequestration of proinflammatory cytokines, Nat. Commun. 111 (2020) 2622, https://doi.org/10.1038/s41467-020-16439-7.
[36] D. Hühn, K. Kantner, C. Geidel, Polymer-coated nanoparticles interacting with proteins and cells: focusing on the sign of the net charge, ACS Nano 74 (2013) 3253–3263, https://doi.org/10.1021/nn3059295.
[37] Y. Wang, K. Zhang, T. Li, Macrophage membrane functionalized biomimetic nanoparticles for targeted anti-atherosclerosis applications, Theranostics 111 (2021) 164–180, https://doi.org/10.7150/thno.47841.
[38] R. Kacimi, J.S. Karliner, F. Koudssi, Expression and regulation of adhesion molecules in cardiac cells by cytokines: response to acute hypoxia, Circ. Res. 825 (1998) 576–586, https://doi.org/10.1161/01.res.82.5.576.
[39] T. Zhang, Y. Zhang, M. Cui, CaMKII is a RIP3 substrate mediating ischemia- and oxidative stress-induced myocardial necroptosis, Nat. Med. 222 (2016) 175–182, https://doi.org/10.1038/nm.4017.
[40] H.B. Suliman, M.S. Carraway, A.S. Ali, The CO/HO system reverses inhibition of mitochondrial biogenesis and prevents murine doxorubicin cardiomyopathy, J. Clin. Invest. 11712 (2007) 3730–3741, https://doi.org/10.1172/jci32967.
[41] M. Bayeva, M. Gheorghiade, H. Ardehali, Mitochondria as a therapeutic target in heart failure, J. Am. Coll. Cardiol. 616 (2013) 599–610, https://doi.org/10.1016/j.jacc.2012.08.1021.
[42] Y.B. Patil, S.K. Swaminathan, T. Sadhukha, The use of nanoparticle-mediated targeted gene silencing and drug delivery to overcome tumor drug resistance, Biomaterials 312 (2010) 358–365, https://doi.org/10.1016/j.biomaterials.2009.09.048.
[43] K. Ying, Y. Zhu, J. Wan, Macrophage membrane-biomimetic adhesive polycaprolactone nanocamptothecin for improving cancer-targeting efficiency and impairing metastasis, Bioact. Mater. 20 (2023) 449–462, https://doi.org/10.1016/j.bioactmat.2022.06.013.
[44] C. Ding, C. Yang, T. Cheng, Macrophage-biomimetic porous Se@SiO(2) nanocomposites for dual modal immunotherapy against inflammatory osteolysis, J. Nanobiotechnol. 191 (2021) 382, https://doi.org/10.1186/s12951-021-01128-4.
[45] C. Zhang, S.Y. Peng, S. Hong, Biomimetic carbon monoxide nanogenerator ameliorates streptozotocin induced type 1 diabetes in mice, Biomaterials 245 (2020), 119986, https://doi.org/10.1016/j.biomaterials.2020.119986.
[46] P.L. Rodriguez, T. Harada, D.A. Christian, Minimal "Self" peptides that inhibit phagocytic clearance and enhance delivery of nanoparticles, Science 3396122 (2013) 971–975, https://doi.org/10.1126/science.1229568.
[47] B.A. Imhof, M. Aurrand-Lions, Adhesion mechanisms regulating the migration of monocytes, Nat. Rev. Immunol. 46 (2004) 432–444, https://doi.org/10.1038/nri1375.
[48] N.G. Frangogiannis, O. Dewald, Y. Xia, Critical role of monocyte chemoattractant protein-1/CC chemokine ligand 2 in the pathogenesis of ischemic cardiomyopathy, Circulation 1155 (2007) 584–592, https://doi.org/10.1161/circulationaha.106.646091.
[49] Y. Wei, M. Zhu, S. Li, Engineered biomimetic nanoplatform protects the myocardium against ischemia/reperfusion injury by inhibiting pyroptosis, ACS Appl. Mater. Interfaces 1329 (2021) 33756–33766, https://doi.org/10.1021/acsami.1c03421.
[50] N. Zhang, Y. Song, Z. Huang, Monocyte mimics improve mesenchymal stem cell-derived extracellular vesicle homing in a mouse MI/RI model, Biomaterials 255 (2020), 120168, https://doi.org/10.1016/j.biomaterials.2020.120168.
[51] L. Tao, E. Gao, X. Jiao, Adiponectin Cardioprotection after Myocardial Ischemia/reperfusion Involves the Reduction of Oxidative/nitrative Stress, vol. 11511, 2007, pp. 1408–1416, https://doi.org/10.1161/circulationaha.106.666941.
[52] L. Tao, X. Jiao, E. Gao, Nitrative inactivation of thioredoxin-1 and its role in postischemic myocardial apoptosis, Circulation 11413 (2006) 1395–1402, https://doi.org/10.1161/circulationaha.106.625061.
[53] J. Clark, P. Naughton, S. Shurey, Cardioprotective actions by a water-soluble carbon monoxide-releasing molecule, Circ. Res. 932 (2003) e2–e8, https://doi.org/10.1161/01.Res.0000084381.86567.08.
[54] G. Wang, T. Hamid, R. Keith, Cardioprotective and antiapoptotic effects of heme oxygenase-1 in the failing heart, Circulation 12117 (2010) 1912–1925, https://doi.org/10.1161/circulationaha.109.905471.
[55] H. Wang, H. Liu, J. Li, Cytokine nanosponges suppressing overactive macrophages and dampening systematic cytokine storm for the treatment of hemophagocytic lymphohistiocytosis, Bioact. Mater. 21 (2023) 531–546, https://doi.org/10.1016/j.bioactmat.2022.09.012.
[56] C. Cai, Z. Guo, X. Chang, Empagliflozin attenuates cardiac microvascular ischemia/reperfusion through activating the AMPKα1/ULK1/FUNDC1/mitophagy pathway, Redox Biol. 52 (2022), 102288, https://doi.org/10.1016/j.redox.2022.102288.